MAPPING THE SHORES OF THE BROWN DWARF DESERT, I: UPPER SCORPIUS

Adam L. Kraus
Department of Astrophysics, California Institute of Technology, Pasadena, CA 91125

Michael J. Ireland
Division of Geological and Planetary Sciences, California Institute of Technology, Pasadena, CA 91125

Frantz Martinache, James P. Lloyd
Department of Astronomy, Cornell University, Ithaca, NY 14853
Draft version February 2, 2008

ABSTRACT

We present the results of a survey for stellar and substellar companions to 82 young stars in the nearby OB association Upper Scorpius. This survey used nonredundant aperture-mask interferometry to achieve typical contrast limits of $\Delta K \sim$5-6 at the diffraction limit, revealing 12 new binary companions that lay below the detection limits of traditional high-resolution imaging; we also summarize a complementary snapshot imaging survey that discovered 7 directly resolved companions. The overall frequency of binary companions ($\sim 35^{+5}_{-4}\%$ at separations of 6-435 AU) appears to be equivalent to field stars of similar mass, but companions could be more common among lower-mass stars than for the field. The companion mass function has statistically significant differences compared to several suggested mass functions for the field, and we suggest an alternate log-normal parameterization of the mass-function. Our survey limits encompass the entire brown dwarf mass range, but we only detected a single companion that might be a brown dwarf; this deficit resembles the so-called "brown dwarf desert" that has been observed by radial-velocity planet searches. Finally, our survey's deep detection limits extend into the top of the planetary mass function, reaching 8-12 M_{Jup} for half of our sample. We have not identified any planetary companions at high confidence ($\gtrsim$99.5%), but we have identified four candidate companions at lower confidence ($\gtrsim$97.5%) that merit additional followup to confirm or disprove their existence.

Subject headings: stars:binaries:general; stars:low-mass,brown dwarfs;stars:pre-main sequence

1. INTRODUCTION

The detection and characterization of low-mass companions has become one of the highest priorities of the astronomical community. Radial velocity surveys have discovered over 200 extrasolar planetary companions over the past decade, and both RV surveys and coronagraphic imaging surveys have discovered an abundance of stellar-mass companions (e.g. Marcy & Butler 2000; McCarthy & Zuckerman 2004; Metchev 2005; Johnson et al. 2006; Naef et al. 2007). However, very few brown dwarf companions have been identified, an unexpected result given that the observational signatures of more massive companions are far larger than those of planetary-mass companions and that free-floating brown dwarfs are very common (Kirkpatrick et al. 2000; Luhman et al. 2003; Chiu et al. 2006; Slesnick et al. 2006a, 2006b). This dearth of companions between the stellar and planetary mass regimes is popularly known as the "brown dwarf desert". The existence and extent of the brown dwarf desert can provide key constraints on star and planet formation since it represents the extreme mass limit of both processes.

If the stellar-mass binary companions of solar-mass stars are drawn from the Initial Mass Function (IMF; e.g. Kroupa 1995) or formed via some other process that preferentially forms low-mass companions (e.g. Duquennoy & Mayor 1991, hereafter DM91), then brown dwarf companions should be common unless another process in-hibits their formation or dynamically strips them. However, if stellar companions are formed via the fragmentation of a protostellar core, then there are no a priori expectations that brown dwarfs should form. Indeed, even if fragmentation can form an extremely inequal-mass pair, the long collapse timescale for low-mass objects might lead to their preferential photoevaporation by the higher-mass, more luminous companion.

It is also unclear whether brown dwarfs could form via planetary formation processes. Radial velocity surveys suggest that the giant planetary mass function is well-fit by a power law, $dN/dm \propto M^{-1.05}$, for masses of $\sim$1-10 M_{Jup} (Marcy et al. 2005). If this power law extends to higher masses, there should be as many "planetary" companions with masses of 10-25 M_{Jup} as with masses of 4-10 M_{Jup} or 1.6-4.0 M_{Jup}. An absence of these companions suggests either that the function is not a power law or that the power law is truncated by some limit. For example, submillimeter disk surveys suggest that proto-planetary disks have a mean mass of $\sim$5 M_{Jup} by the age of 1-2 Myr (Andrews & Williams 2005), with a small fraction ($\sim$5%) having masses of $\sim$30-100 M_{Jup}. Unless massive planets are formed very early or efficiently accrete the entire disk mass, this could impose an upper cutoff on the distribution of planetary masses.

The brown dwarf desert has been studied mostly at very small or very large separations. The radial velocity exoplanet surveys that have proven so successful

over the past decade should have detected any brown dwarfs within their outer separation limit ($\sim$3-5 AU), and they have set very low upper limits on the frequency of close brown dwarf companions to solar mass stars ($<$1%; Marcy & Butler 2000; Grether & Lineweaver 2006). Similarly, high-resolution coronagraphic imaging surveys have demonstrated sufficient sensitivity to identify brown dwarf companions at typical separation limits of $>$50 AU (e.g. Gizis et al. 2001; Neuhäuser et al. 2003; McCarthy & Zuckerman 2004; Neuhäuser & Guenther 2004; Metchev 2005). They have measured frequencies which are low, but somewhat inconsistent (and perhaps not anomalously low; 1$\pm$1% by McCarthy & Zuckerman, compared to $6.8^{+8.3}_{-4.9}$% by Metchev and 18$\pm$14% by Gizis et al.). A survey for wide companions to high-mass (2-8 $M_\odot$) stars in Upper Sco by Kouwenhoven et al. (2007) found a relatively low frequency for brown dwarf companions, 0.5$\pm$0.5% at separations of 130-520 AU. Finally, there have been an intriguing sample of candidate planetary-mass companions identified at large separations (e.g. Chauvin et al. 2004; Neuhäuser et al. 2005), but both their mass and formation mechanism are still uncertain and their frequency is still unconstrained (e.g. Masciadri et al. 2005; Kraus et al. 2006; Biller et al. 2007; Ahmic et al. 2007).

However, these surveys don't study the actual separation range where most giant planets and binary companions are expected to form. Most giant planets at small orbital radii ($\lesssim$5 AU) are thought to have migrated inward, so their mass distribution may not match that of their more distant brethren. The binary formation process may also be different for small separations ($\lesssim$10 AU), with H_2 dissociation softening the equation of state and leading to enhanced fragmentation over that expected for larger length scales (Whitworth & Stamatellos 2006). Similarly, giant planets aren't expected to form at very large radii ($\gtrsim$30 AU) since the formation timescale is too long, and the frequency of wide binary companions may differ significantly from those of closer binaries (e.g. Kraus & Hillenbrand 2007a) since the fragmentation occurs on a length scale that is several orders of magnitude larger.

Ideally, the desert should be studied at the separation range where giant planets and most binaries are thought to form ($\sim$5-30 AU; Lissauer & Stephenson 2007; DM91), but this has been impossible using existing techniques. For example, theoretical models (Chabrier et al. 2000) suggest that a 50 M_{Jup} brown dwarf located 15 AU (1-2$''$) from a nearby field star will have a contrast ratio of $\Delta K \sim$10-15 magnitudes at a separation of only $\sim$1$''$. The contrast problem could have been addressed by observing young stars since their substellar companions would be intrinsically more luminous ($\Delta K <$5 mag), but most young stars are further away, so the separations are even smaller (0.1-0.2$''$; $\sim\lambda/D$). Sensitivities near the diffraction limit have traditionally been far too shallow to detect such companions. However, new advances in high-resolution imaging techniques are now opening up this critical regime; our survey will use one such technique, non-redundant aperture mask interferometry.

The technique of non-redundant aperture masking has been well-established as a means of achieving the full diffraction limit of a single telescope (e.g. Nakajima et al.

1989; Tuthill et al. 2000). The reason for the technique's success over direct imaging is that the calibration is independent of structure of the wavefront over scales larger than a single sub-aperture, but it still preserves the angular resolution of the full aperture. This technique, when applied to seeing-limited observations, requires observations to be taken in a speckle mode with sub-apertures of diameter smaller than the atmospheric coherence length, limiting the technique to objects brighter than about $m_H = 5$. The use of adaptive optics allows for longer integration times and larger sub-apertures, extending the technique to much fainter targets.

Published detections have been able to recover astrometrically discovered binary systems with contrast ratios of 3:1 at 0.6 λ/D and 100:1 at λ/D (Pravdo et al. 2006; Lloyd et al. 2006; Ireland et al. 2008) using total observation times of $\sim$10 minutes. The inner limit of companion detectability at high contrast is $\lambda/2B_L$, where B_L is the longest baseline in the mask (typically 80-95% of the aperture diameter). Typical closure phase errors are such that aperture masking can unveil high contrast companions at separations 5 times closer than direct imaging in both H and K bands.

In this paper, we describe an aperture-mask interferometry and direct imaging survey to detect stellar and substellar companions to young stars in the nearby OB association Upper Scorpius. This survey directly studies the age and separation range corresponding to the peak of planet formation, offering the first glimpse of the brown dwarf desert in this critical range of parameter space. In Section 2, we describe our survey sample, and in Section 3, we describe the observations and data analysis techniques. In Section 4, we summarize the results of our survey. In Section 5, we combine these results with previous binary surveys to place constraints on the stellar binary frequency, mass function, and separation distribution, and in Section 6, we consider constraints on the corresponding parameters for the planetary population. Finally, in Section 7, we discuss the implications of our survey for the extent and aridity of the brown dwarf desert.

2. SURVEY SAMPLE

Upper Sco is an ideal target for large-scale surveys to detect brown dwarf or planetary companions. It is young enough ($\sim$5 Myr) that substellar companions are much more luminous than those of typical field stars, and this age is thought to be the peak epoch of giant planet formation (Lissauer & Stephenson 2007, and references therein). Its relative proximity ($\sim$145 pc; de Zeeuw et al. 1999) also means that the resolution limit of large telescopes ($\sim$40-100 mas; 6-15 AU) corresponds to the giant planet separation regime of our own solar system. Finally, the association has been very intensely studied, with several hundred members identified in the past decade, so it provides a much larger sample of well-characterized members than nearby moving groups.

We compiled a preliminary list of 356 targets from the known members of Upper Sco as compiled in Kraus & Hillenbrand (2007a); this census included all spectroscopically-confirmed members with spectral type G0 or later from the recent surveys by Walter et al. (1994), Preibisch et al. (1998, 2001, 2002), Kunkel (1999), Ardila et al. (2000), Martin et al. (2004),

and Slesnick et al. (2006a). We also added two stars that were not included in that census: RXJ1550.9-2534 (which was originally classified as F9 by the HD catalogue but was reclassified as G1 by the Michigan Spectral Survey; Houk & Smith-Moore 1988) and V1149 Sco (which was not included in any large membership surveys since it was identified as a young star before they were conducted; Stephenson 1986).

All of our observations have been conducted from northern sites, so we removed 25 of the 26 stars south of $\delta = -25^o$ from further consideration. The only exception was RXJ1550.9-2534, which we retained in order to make a complete group of four science targets of similar brightness and airmass. As we describe below, preliminary imaging showed that it was an obvious binary that is not suitable for masking observations anyway, but we retain it in our sample for statistical purposes. We also rejected 230 of the remaining low-mass association members which were optically fainter than the useful limit of the AO system ($R \gtrsim 14$). Finally, we removed the 23 known binaries with separations of $<3''$. In close systems, the stellar companion would have dominated the signal in our observations, complicating any search for fainter companions. Wider binaries (with separations near the seeing limit) were rejected because they are generally not corrected well by the AO system, though we still observed several of them with direct imaging in order to test whether this would actually occur. A total of seven targets were not discovered to be binaries until we arrived at the telescope and obtained quick direct imaging observations; these targets were also removed from the aperture mask sample. We mistakenly removed one more target, USco-160643.8-190805, that we initially thought was a binary based on direct imaging. Subsequent analysis showed that it was flagged as a binary erroneously; we will not consider it in our statistical sample because we only have imaging data and not masking data.

These cuts left a total of 72 Upper Sco members in our aperture mask sample, plus 11 members (10 known or new binary systems and 1 erroneous omission) that we only observed with direct imaging. We list all of these targets in Table 1, where we also include each target's spectral type (adopted from the discovery survey), mass (as determined in Section 3.3), and R and K magnitudes, plus the target group that it was observed with (as described in Section 3.1). In Table 2, we list the 19 known binary systems that would have passed our selection criteria. We did not observe any of these systems, but we will include them in our sample for determining stellar binary statistics since they have known binary companions. Our upper limits on the existence of planetary-mass companions will not include any known or newly-discovered binary systems.

3. OBSERVATIONS AND DATA ANALYSIS

3.1. Observations

We observed our target sample in April-July 2007 with the Keck-II 10m and Palomar Hale 200" telescopes. All observations were obtained using the facility adaptive optics imagers, NIRC2 and PHARO. Both instruments have aperture masks permanently installed at or near the pupil plane in filter or pupil-stop wheels. The seeing quality was well above average for most of the Keck observations, yielding superb AO correction for bright targets and acceptable strehl ratios ($\sim$15-20%) even for targets as faint as $R \sim 14$. The Palomar observations were obtained under approximately median conditions ($\sim 1''$ seeing).

All observations conducted at Keck were obtained with a K' filter, while those conducted at Palomar were obtained with a methane short filter, which is in H-band (central wavelength $1.57\,\mu$m, bandpass $0.1\,\mu$m). This filter was used instead of full H-band because of calibration errors related to dispersion that had been found in previous data sets. This strategy allowed us to achieve similar resolution limits at both telescopes, despite the smaller aperture size at Palomar. Our Palomar observations suffered a modest loss of sensitivity since the strehl is lower in H than in K', but the typical sensitivity limit in H still allows us to detect a $\sim 30\,M_{Jup}$ companion at 40 mas for half of our sample members. Observing in K would have yielded limits of $\Delta K \lesssim 1$ magnitude deeper (equivalent to $\Delta H \lesssim 1.5$ since low-mass companions are redder in $H - K$), and we decided this was not as important since the corresponding detection limits ($\gtrsim$15-20 M_{Jup}) could not have reached the planetary mass range.

Observations at Keck used a 9 hole mask, with the longest baseline 8.27 m and the shortest baseline 1.67 m. We used a multiple-correlated double sampling readout in a 512x512 subarray of the ALADDIN detector, with 16 endpoint reads and a 10 s exposure per frame. Observations at Palomar with PHARO also used a 9 hole mask, with the longest baseline 3.94 m and the shortest baseline 0.71 m. To maximise the number of reads, we used either a 256x256 or 150x150 sub-array mode in one quadrant of the HAWAII detector, with a total of 16 or 28 reads respectively per array reset. Every read was saved to disk, so that in post-processing each file could be split into sub-frames. Splitting the data into more sub-frames minimises sensitivity to changing seeing or AO instabilities, and using less sub-frames minimises sensitivity to readout noise. We found that for the typical magnitudes of our targets, signal-to-noise was optimized by using read pairs separated by one read: giving 862 ms exposure times for the 256x256 sub-array mode, and 430 ms exposure times for the 150x150 sub-array mode.

A key requirement for obtaining good contrast limits is the contemporaneous observation of calibrator sources, ideally single stars which are nearby on the sky and similar in both optical and near-infrared brightness. A typical observing mode for isolated field stars is to obtain several sets of observations for a science target, interspersing visits to calibrator stars between each science observation. As a result, observations for a single science target might require as many as six target acquisitions (three calibrators, plus three visits to the source). However, all of our science targets are located in close proximity on the sky ($<10^o$) and they span a continuous range of brightness, so we were able to use the same calibrator star for multiple science targets and to inter-calibrate between science targets. To this end, we divided our sample into 20 groups of $\sim$4 similar-brightness stars each, then observed each group contemporaneously. Specifically, we visited each group member three times, plus we obtained one visit for each of two independent field calibrators. This allowed us to typically observe four science targets with a total of 14 acquisitions, for an

TABLE 1
Upper Sco sample

Name	RA	DEC	SpT	Mass ($M_\odot$)	R (mag)	K (mag)	Group
	(J2000)						
RXJ1550.0-2312	15 50 04.99	-23 11 53.7	M2	0.49	13.1	8.93	14
RXJ1550.9-2534	15 50 56.42	-25 34 19.0	G1	1.75	9.4	7.91	...
RXJ1551.1-2402	15 51 06.61	-24 02 19.0	M2	0.49	13.5	9.73	17
RXJ1557.8-2305	15 57 50.03	-23 05 09.4	M0	0.68	12.7	9.27	12
RXJ1558.1-2405	15 58 08.15	-24 05 53.0	K4	0.95	11.4	8.96	8
RXJ1558.2-2328	15 58 12.71	-23 28 36.4	G2	1.66	9.9	8.02	1
RXJ1600.2-2417	16 00 13.30	-24 18 10.6	M0	0.68	13.1	9.51	14
RXJ1600.6-2159	16 00 40.57	-22 00 32.2	G9	1.43	10.2	8.44	3
RXJ1600.7-2127	16 00 42.77	-21 27 38.0	K7	0.77	11.7	8.92	10
RXJ1601.1-2113	16 01 08.01	-21 13 18.5	M0	0.68	12.0	8.80	9
RXJ1601.9-2008	16 01 58.23	-20 08 12.2	G5	1.62	9.9	7.67	2
RXJ1602.0-2221	16 02 00.39	-22 21 23.7	M1	0.60	12.8	8.84	12
RXJ1602.8-2401B	16 02 51.24	-24 01 57.4	K4	0.95	11.1	8.93	4
RXJ1602.8-2401A	16 02 52.43	-24 02 22.7	K0	1.35	10.4	7.65	1
RXJ1603.6-2245	16 03 35.50	-22 45 56.1	G9	1.43	10.6	8.36	3
RXJ1603.9-2031A	16 03 57.68	-20 31 05.5	K5	0.87	12.0	8.37	10
RXJ1604.3-2130	16 04 21.66	-21 30 28.4	K2	1.12	11.8	8.51	11
RXJ1605.6-2152	16 05 39.36	-21 52 33.8	M1	0.60	13.6	9.47	17
RXJ1606.2-2036	16 06 12.54	-20 36 47.3	K5	0.87	12.5	8.90	12
RXJ1607.0-2043	16 07 03.73	-20 43 07.4	M1	0.60	13.6	9.53	17
RXJ1607.0-2036	16 07 03.56	-20 36 26.5	M0	0.68	11.3	8.10	...
USco-155655.5-225839	15 56 55.46	-22 58 40.4	M0	0.68	13.2	9.43	14,15
USco-160142.6-222923	16 01 42.55	-22 29 23.9	M0	0.68	13.8	10.22	19
USco-160341.8-200557	16 03 41.87	-20 05 57.8	M2	0.49	13.7	9.49	18
USco-160343.3-201531	16 03 43.35	-20 15 31.5	M2	0.49	13.7	9.72	18
Usco-160428.4-190441	16 04 28.39	-19 04 41.4	M3	0.36	13.6	9.28	...
USco-160517.9-202420	16 05 17.92	-20 24 19.5	M3	0.36	13.3	9.14	15
USco-160643.8-190805	16 06 43.86	-19 08 05.6	K6	0.82	12.8	9.20	...
USco-160707.7-192715	16 07 07.67	-19 27 16.1	M2	0.49	13.8	9.80	19
USco-160801.4-202741	16 08 01.42	-20 27 41.7	K8	0.68	13.0	9.29	16
USco-160822.4-193004	16 08 22.34	-19 30 05.2	M1	0.60	12.9	9.06	12
USco-160823.2-193001	16 08 23.25	-19 30 00.9	K9	0.68	13.2	9.47	15
USco-160823.8-193551	16 08 23.88	-19 35 51.8	M1	0.60	13.3	9.25	...
USco-160825.1-201224	16 08 25.11	-20 12 24.6	M1	0.60	13.9	9.87	20
USco-160900.7-190852	16 09 00.76	-19 08 52.6	K9	0.68	13.1	9.15	15
USco-160908.4-200928	16 09 08.45	-20 09 27.8	M4	0.24	13.8	9.52	...
USco-160916.8-183522	16 09 16.85	-18 35 22.6	M2	0.49	14.0	9.67	20
USco-160946.4-193735	16 09 46.44	-19 37 36.1	M1	0.60	13.8	9.63	19
USco-160954.4-190654	16 09 54.41	-19 06 55.1	M1	0.60	13.7	9.60	18
USco-161031.9-191305	16 10 31.96	-19 13 06.2	K7	0.77	13.0	8.99	12
USco-161115.3-175721	16 11 15.34	-17 57 21.4	M1	0.6	13.2	9.20	15
USco-161347.5-183459	16 13 47.51	-18 35 00.4	M2	0.49	14.1	9.91	20
USco-161358.1-184828	16 13 58.15	-18 48 29.0	M2	0.49	14.0	9.88	20
GSC 06764-01305	15 35 57.80	-23 24 04.6	K3	0.99	12.0	9.43	11
GSC 06195-00768	15 57 02.34	-19 50 42.0	K7	0.77	11.1	8.37	...
GSC 06191-00019	15 59 02.09	-18 44 14.3	K6	0.82	11.1	8.11	...
GSC 06191-00552	15 58 47.70	-17 57 59.0	K3	0.99	11.5	8.33	5
GSC 06204-00812	16 03 02.69	-18 06 05.0	K4	0.95	11.3	8.73	5
GSC 06204-01067	16 03 23.68	-17 51 42.3	M2	0.49	12.4	8.61	...
GSC 06208-00834	16 06 31.70	-20 36 23.3	K6	0.82	12.4	8.73	10
GSC 06209-00735	16 08 14.74	-19 08 32.8	K2	1.12	11.0	8.43	5
GSC 06205-00954	16 08 31.38	-18 02 41.4	M0	0.68	12.2	8.91	9
GSC 06209-01501	16 08 56.73	-20 33 46.0	K5	0.87	11.9	8.62	9
GSC 06213-01358	16 09 30.30	-21 04 58.9	M0	0.68	12.1	8.92	9
GSC 06213-00194	16 09 40.99	-22 17 59.4	M0	0.68	11.6	8.44	7
GSC 06213-00306	16 10 42.03	-21 01 32.0	K5	0.87	11.9	8.56	6
GSC 06793-00868	16 11 56.33	-23 04 05.1	M1	0.6	12.2	8.82	...
GSC 06793-00797	16 13 02.72	-22 57 44.6	K4	0.95	11.7	8.46	8
GSC 06213-00306	16 13 18.59	-22 12 48.9	G9	1.43	9.8	7.43	1,2
GSC 06793-00994	16 14 02.12	-23 01 02.2	G4	1.63	10.9	8.61	4
GSC 06793-00806	16 15 34.57	-22 42 42.1	M1	0.60	11.2	7.91	7
GSC 06793-01406	16 16 17.95	-23 39 47.7	G7	1.56	9.9	8.10	2
GSC 06214-02384	16 19 33.96	-22 28 29.4	K0	1.35	10.5	8.51	3
GSC 06794-00480	16 20 45.96	-23 48 20.9	K3	0.99	11.9	8.93	8
GSC 06214-00210	16 21 54.67	-20 43 09.1	M1	0.60	11.6	9.15	8
GSC 06794-00537	16 23 07.83	-23 00 59.7	K2	1.12	11.0	8.18	4
GSC 06794-00156	16 24 51.36	-22 39 32.5	G6	1.59	9.3	7.08	1
GSC 06794-00337	16 27 39.56	-22 45 23.0	K1	1.25	10.9	8.08	6
GSC 06228-01359	16 35 48.36	-21 48 39.7	M0	0.68	12.4	8.48	10
ScoPMS015	15 57 19.99	-23 38 50.0	M0	0.68	12.4	8.88	...
ScoPMS017	15 57 34.31	-23 21 12.3	M1	0.60	12.9	8.99	14
ScoPMS019	15 59 59.95	-22 20 36.8	M1	0.60	12.3	8.63	11
ScoPMS021	16 01 25.64	-22 40 40.3	K1	1.25	13.6	8.52	16
ScoPMS022	16 02 08.45	-22 54 58.9	M1	0.60	13.4	9.55	17
ScoPMS027	16 04 47.76	-19 30 23.1	K2	1.12	11.0	8.04	5
ScoPMS028	16 05 27.27	-19 38 46.6	M1	0.60	13.3	9.55	16
ScoPMS042b	16 10 21.74	-19 04 06.7	M3	0.36	13.8	9.62	19
ScoPMS044	16 11 08.91	-19 04 46.9	K2	1.12	11.3	7.69	7
ScoPMS045	16 11 20.58	-18 20 54.9	K5	0.87	11.4	8.56	6

TABLE 2
Known Binary Systems

Primary	RA	DEC	SpT$_{prim}$	M_{prim}	R	K	ΔK	Sep	PA	Ref
	(J2000)			($M_\odot$)	(mag)	(mag)	(mag)	(mas)	(deg)	
GSC 06780-01061	16 06 54.36	-24 16 10.8	M3	0.36	12.2	8.86	1.3	1500	270.0	Kraus & Hillenbrand (2007a)
GSC 06793-00569	16 13 29.29	-23 11 07.5	K1	1.25	11.1	8.49	2.7	1430	91.4	Metchev (2005)
GSC 06793-00819	16 14 11.08	-23 05 36.2	K0	1.35	10.0	7.46	0.21	222	304.8	Metchev (2005)
RXJ1600.5-2027	16 00 31.35	-20 27 05.0	M1	0.60	12.8	8.83	0.43	189	171.7	Köhler et al. (2000)
RXJ1601.7-2049	16 01 47.43	-20 49 45.8	M0	0.68	12.4	8.61	0.58	205	324.7	Köhler et al. (2000)
RXJ1601.8-2445	16 01 51.49	-24 45 24.9	K7	0.77	11.4	8.49	1.00	76	289.6	Köhler et al. (2000)
RXJ1602.9-2022	16 02 53.96	-20 22 48.1	K7	0.77	11.7	8.19	0.18	310	5.3	Köhler et al. (2000)
RXJ1603.9-2031B	16 03 54.96	-20 31 38.4	M0	0.68	12.5	8.62	0.53	121	140.9	Köhler et al. (2000)
RXJ1606.6-2108	16 06 37.41	-21 08 40.5	M1	0.60	13.2	9.11	0.09	1279	33.9	Köhler et al. (2000)
RXJ1607.0-1911	16 07 03.94	-19 11 33.9	M1	0.60	13.4	9.22	1.47	599	87.6	Köhler et al. (2000)
ScoPMS005	15 54 59.86	-23 47 18.2	G2	1.66	8.6	7.03	1.99	766	232.0	Köhler et al. (2000)
ScoPMS013	15 56 29.42	-23 48 19.8	M1.5	0.54	11.6	8.75	0.62	92	169.8	Köhler et al. (2000)
ScoPMS016	15 57 25.76	-23 54 22.0	M0.5	0.64	13.1	9.09	0.63	1324	226.0	Köhler et al. (2000)
ScoPMS020	16 01 05.19	-22 27 31.2	M3	0.36	12.9	8.75	0.60	193	313.7	Köhler et al. (2000)
ScoPMS023	16 02 10.45	-22 41 28.0	K5	0.87	10.2	8.06	0.65	300	345.6	Köhler et al. (2000)
ScoPMS029	16 05 42.67	-20 04 15.0	M2	0.49	13.4	9.16	0.56	643	352.6	Köhler et al. (2000)
ScoPMS031	16 06 21.96	-19 28 44.6	M0.5	0.64	12.8	8.62	0.64	578	148.2	Köhler et al. (2000)
ScoPMS042a	16 10 28.58	-19 04 47.0	M1	0.60	13.0	8.71	0.42	299	84.1	Köhler et al. (2000)
ScoPMS052	16 12 40.51	-18 59 28.3	K0	1.35	10.4	7.49	1.10	144	162.2	Metchev (2005)

NOTE. — Typical uncertainties are ∼1 subclass for spectral types, ∼0.2 mag for R magnitudes (taken from NOMAD; Zacharias et al. 2004), and ∼0.02 mag for K magnitudes (taken from 2MASS; Skrutskie et al. 2006). The uncertainties in masses are dominated by systematic errors, including a global zero-point uncertainty of ∼20% and individual uncertainties of as much as ∼100% due to the possibility of further unresolved multiplicity. Typical uncertainties in binary properties are ∼0.1 mag in ΔK, ∼10 mas in separation, and ∼1 deg in PA.
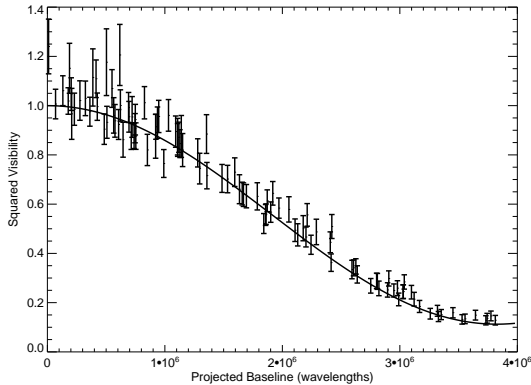
Fig. 1.— The squared visibilities as a function of projected baseline for the 27 mas binary RXJ1550.0-2312. Despite a separation of only 0.6 λ/D, the binary system is clearly detected; the solid line denotes our best-fit value for the system parameters (Table 5).
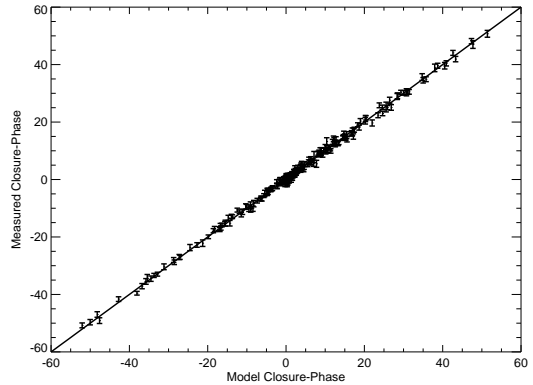

Fig. 2.— The measured close phases as a function of modeled closure phases for RXJ1550.0-2312, assuming that it has the best-fit parameters that we list in Table 5 (a 27 mas binary with a flux ratio of 2:1).

average of 3.5 acquisitions per target. The average total time per acquisition was ∼4 minutes, so our strategy required ∼15 minutes per target.

We summarize the composition of our target groups and list the independent calibrators in Table 3. We also include the observation date and the mean R and K magnitudes for each group. Some of our groups are bigger or smaller because our acquisition images showed that several intended targets were resolved binaries (Section 3.3). When this occurred, we removed the binary system from our sample; in the case of Groups 12-15, we found a large number of binaries, so we rearranged the group composition at the telescope and eliminated Group 13.

Finally, a large fraction of our sample has been observed previously with high-resolution imaging (Brandner et al. 1996; Metchev 2005; Bouy et al. 2006), so we knew a priori whether these stars had known companions. However, many of our targets have been observed only with speckle imaging (Köhler et al. 2000) or have not been observed with any high-resolution techniques. For these sources, we decided to obtain quick observations in direct-imaging mode in order to screen out obvious binaries. This also allowed us to test for companions at separations outside the nominal limit of aperture-mask interferometry (240 mas at Palomar and 320 mas at Keck).

In Table 4, we list all of the sources that were observed with direct imaging and summarize the observations. We observed all of these sources with NIRC2 or PHARO using the smallest pixel scale available (10 or 25 mas pix^{-1}, respectively) and a two-point diagonal dither pattern. Faint stars were observed with a K' or K_s filter, while bright stars that would have saturated the detector were observed with a $Br\gamma$ filter, which attenuates flux by a factor of ∼10 relative to broadband K filters.

3.2. Aperture Mask Analysis and Detection Limits

The aperture-masking analysis pipeline is similar to that used for several previous papers containing Palomar masking data (Pravdo et al. 2006; Lloyd et al. 2006; Martinache et al 2007). After subtracting the bias (dark) level, flat-fielding and removing bad pixels, the data are windowed by a super-Gaussian (a function of the form $\exp(-kx^4)$). This window both limits sensitivity to readout noise and acts as a spatial-filter. Each

frame is then Fourier-transformed, and the complex visibility extracted for each baseline. Complex visibilities cannot be directly used for high-fidelity measurements because of their sensitivity to variable optical aberrations and non common path errors. Instead, we use the averaged squared visibility and the complex triple product (Lohmann et al. 1983). For each visit to each star, we extract squared-visibility, closure-phase, and the uncertainties on these quantities based on the scatter within one visit. Finally, the calibration process consists of estimating the instrumental squared-visibilities and closure-phases. The target star's squared visibilities are divided by the instrumental squared-visibilities and the instrumental closure-phase is subtracted from the measured closure-phase.

Figures 1 and 2 show a fit to data for the 27 mas separation binary RXJ1550.0-2312. Squared visibility is plotted against baseline projected along the axis of the binary. As closure-phase is a multi-dimensional quantity, we chose to simply plot the measured closure-phases versus the model closure-phases. Despite this binary being at a separation of only $0.6\lambda/D$, it is clear that it is an extremely-high signal-to-noise detection. Note that only closure-phase was used in the fit: calibration errors are evident in the squared visibility data with the few points that have squared visibility greater than 1.0.

The error analysis procedure used to calculate the covariance matrix of closure-phase for each target is given in detail in Appendix A. For all targets, an attempt at fitting a binary solution was made, by first searching exhaustively in a grid in position angle and separation at high-contrast and then by a gradient descent search to find the χ^2 minimum. Errors in binary parameters were calculated from the curvature of the χ^2 surface at the χ^2 minimum (i.e. the same method as most least-squares algorithms). Detections were retained if their contrast was greater than a 99.9% confidence threshold.

In order to calculate a detection threshold, we simulated 10000 data sets with the identical (u, v)-sampling and error properties of each target. For each of these simulated data sets, we calculated the best fit contrast ratio for every value of separation and position angle in a large grid, and then tabulated the maximum contrast ratio (i.e. brightest fitted companion) within a series of annuli. Our 99.9% upper limits to companion brightness

TABLE 3
Aperture Mask Observations

Group	Science Targets	Calibrator Stars	Telescope	R (mag)	K (mag)	Epoch (JD-2450000)
1	GSC 06213-00306, GSC 06794-00156 RXJ1558.2-2328, RXJ1602.8-2401A	2M1618-2245, 2M1613-2218	Keck	9.3-10.4	7.08-8.02	4257
2	GSC 06213-00306, GSC 06793-01406 RXJ1601.9-2008, ScoPMS060	2M1602-1945, 2M1617-2320	Palomar	9.7-9.9	7.43-8.10	4251
3	GSC 06214-02384, RXJ1600.6-2159 RXJ1603.6-2245, V1149 Sco	2M1559-2303, 2M1620-2231	Palomar	10.2-10.6	7.05-8.36	4252
4	GSC 06793-00994, GSC 06794-00537 RXJ1602.8-2401B, ScoPMS214	2M1613-2311, 2M1630-2118	Palomar	10.5-11.1	7.76-8.93	4312
5	GSC 061901-00552, GSC 06204-00812 GSC 06209-00735, ScoPMS027	2M1558-1747, 2M1606-1924	Palomar	11.0-11.5	8.04-8.73	4250
6	GSC 06213-00306, GSC 06794-00337 ScoPMS045	2M1610-1818, 2M1629-2245	Palomar	10.9-11.9	8.08-8.56	4251
7	GSC 06213-00194, GSC 06793-00806 ScoPMS044, ScoPMS048 A	2M1609-2216, 2M1611-1906	Palomar	11.1-11.6	7.69-8.44	4252
8	GSC 06793-00797, GSC 06794-00480 GSC 06214-00210, RXJ1558.1-2405	2M1622-2036, 2M1558-2412	Palomar	11.4-11.9	8.46-9.15	4252
9	GSC 06205-00954, GSC 06209-01501 GSC 06213-01358, RXJ1601.1-2113	2M1601-2123, 2M1608-2022	Palomar	11.9-12.2	8.62-8.92	4250
10	GSC 06208-00834, GSC 06228-01359 RXJ1600.7-2127, RXJ1603.9-2031A	2M1602-2133, 2M1635-2204	Palomar	11.7-12.4	8.37-8.92	4250
11	GSC 06764-01305, GSC 06793-00868 RXJ1604.3-2130, ScoPMS019	2M1613-2303, 2M1535-2330	Keck	11.8-12.3	8.51-9.43	4257
12	RXJ1557.8-2305, RXJ1602.0-2221 RXJ1606.2-2036, USco-160822.4-193004 USco-161031.9-191305	2M1608-1916	Keck	12.4-13.0	8.61-9.27	4257
14	RXJ1550.0-2312, RXJ1600.2-2417 ScoPMS017, USco-155655.5-225839	2M1600-2421, 2M1543-1929	Keck	12.8-13.0	8.99-9.29	4256
15	USco-155655.5-225839, USco-160517.9-202420 USco-160823.2-193001, USco-160900.7-190852 USco-161115.3-175721	2M1557-2251, 2M1611-1802	Keck	13.1-13.3	9.14-9.47	4257
16	ScoPMS021, ScoPMS028 USco-160801.4-202741, USco-160823.8-193551	2M1606-1949, 2M1607-2027 2M1601-2227	Keck	13.3-13.6	8.52-9.55	4257
17	RXJ1551.1-2402, RXJ1605.6-2152 RXJ1607.0-2043, ScoPMS022	2M1550-2412, 2M1607-2050	Keck	13.4-13.6	9.47-9.73	4256
18	USco-160341.8-200557, USco-160343.3-201531 USco-160908.4-200928, USco-160954.4-190654	2M1610-1904, 2M1614-1846	Keck	13.7-13.8	9.49-9.72	4256
19	ScoPMS042b, USco-160142.6-222923 USco-160707.7-192715, USco-160946.4-193735	2M1602-2229, 2M1607-1929	Keck	13.8-13.8	9.62-10.22	4256
20	USco-160825.1-201224, USco-160916.8-183522 USco-161347.5-183459, USco-161358.1-184828	2M1614-1846, 2M1608-2008	Keck	13.9-14.1	9.67-9.91	4256

within each annulus was taken to be the contrast ratio where 99.9% of the simulations had no fitted companion brighter than this limit anywhere within the annulus. Details of the simulation and fitting algorithms can be found in the Appendix A.

3.3. Imaging Analysis and Detection Limits

The imaging data were flat-fielded and dark- and bias-subtracted using standard IRAF procedures. We measured PSF-fitting photometry and astrometry for our sources using the IRAF package DAOPHOT (Stetson 1987), and specifically with the ALLSTAR routine. Where possible, we analyzed each frame separately in order to estimate the uncertainty in individual measurements and to allow for the potential rejection of frames with inferior AO correction; our final results represent the mean value for all observations in a filter. If the companion could not be easily distinguished in a single filter, we measured photometry from the coadded sum of all images at each dither position.

In all cases, we used the science target (or the primary star of a binary) to produce an analytic PSF composed of a gaussian core with lorentzian wings. If the science target was a close binary, we reconstructed the PSF using the algorithm described in Kraus & Hillenbrand (2007b), which iteratively fits a template PSF to the primary and then subtracts the secondary to fit an improved estimate of the primary. Three sources appeared to be marginally detected in our observations; we retained these sources in our aperture mask sample and later confirmed their multiplicity (Section 4), so we processed their images with our PSF reconstruction routine and report the results. Finally, we calibrated our photometry using the known 2MASS K_s magnitudes for each of our science targets; these absolute magnitudes are uncertain by $\sim$0.1-0.2 magnitudes due to the intrinsic variability of young stars (resulting from accretion or rotation).

At small separations ($\lesssim 5\lambda/D$), our imaging data for apparently single stars will be superceded by our aperture mask data, so the detection limits are not important. At larger separations ($\gtrsim 5\lambda/D$), where spurious sources corresponding to AO speckles dominate, we adopted the detection limits suggested by Metchev (2005) for similar observations: $\Delta K = 4$ at 250-500 mas, $\Delta K = 5$ at 500-1000 mas, and the sky background limit ($K \sim$16.5-17.5) at separations of $\gtrsim 1''$. We tested these limits for a set of the apparently single stars in our sample by subtracting an analytic PSF from the science target, then compiling the statistics for all apparently spurious detections. In

TABLE 4
Direct Imaging Observations

Name	Telescope	T_{int} (s)	Filter	Epoch (JD-2450000)
GSC 06191-00019	Pal	56.64	Ks	4251
GSC 06195-00768	Pal	18.41	Ks	4199
GSC 06204-01067	Pal	56.64	Ks	4252
GSC 06205-00954	Pal	56.64	Ks	4250
GSC 06208-00834	Pal	56.64	Ks	4250
GSC 06209-01501	Pal	56.64	Ks	4250
GSC 06213-00194	Pal	56.64	Ks	4251
GSC 06213-00306	Pal	56.64	Ks	4251
GSC 06213-01358	Pal	56.64	Ks	4250
GSC 06214-00210	Pal	56.64	Ks	4251
GSC 06214-02384	Pal	56.64	Ks	4251
GSC 06764-01305	Pal	56.64	Ks	4252
GSC 06793-00797	Pal	56.64	Ks	4251
GSC 06793-00806	Pal	56.64	Ks	4251
GSC 06793-00868	Pal	56.64	Ks	4252
GSC 06793-00994	Pal	56.64	Ks	4251
GSC 06794-00156	Pal	56.64	Ks	4251
GSC 06794-00480	Pal	56.64	Ks	4251
GSC 06794-00537	Pal	56.64	Ks	4251
RXJ1550.0-2312	Keck	32	Brg	4256
RXJ1550.0-2312	Keck	32	Brg	4257
RXJ1550.9-2534	Keck	32	Brg	4257
RXJ1551.1-2402	Keck	32	Brg	4256
RXJ1557.8-2305	Keck	32	Brg	4257
RXJ1558.1-2405	Pal	56.64	Ks	4252
RXJ1558.2-2328	Pal	56.64	Ks	4251
RXJ1600.7-2127	Pal	56.64	Ks	4250
RXJ1601.1-2113	Pal	56.64	Ks	4250
RXJ1601.9-2008	Pal	56.64	Ks	4251
RXJ1602.0-2221	Keck	32	Brg	4257
RXJ1602.8-2401A	Keck	16	Brg	4257
RXJ1602.8-2401B	Pal	56.64	Ks	4251
RXJ1603.6-2245	Pal	56.64	Ks	4251
RXJ1603.9-2031A	Pal	56.64	Ks	4250
RXJ1604.3-2130	Pal	56.64	Ks	4252
RXJ1606.2-2036	Pal	56.64	Ks	4252
RXJ1607.0-2036	Pal	56.64	Ks	4251
ScoPMS015	Pal	56.64	Ks	4250
ScoPMS017	Keck	32	Brg	4256
ScoPMS019	Pal	56.64	Ks	4252
ScoPMS022	Keck	32	Brg	4256
ScoPMS027	Pal	28.32	Ks	4250
ScoPMS028	Keck	32	Brg	4257
ScoPMS042b	Keck	44	Brg	4256
ScoPMS044	Pal	56.64	Ks	4251
ScoPMS045	Pal	56.64	Ks	4251
ScoPMS048	Pal	56.64	Ks	4251
USco-160341.8-200557	Keck	32	Brg	4256
Usco-160428.4-190441	Keck	32	Brg	4257
USco-160517.9-202420	Keck	32	Brg	4257
USco-160643.8-190805	Pal	56.64	Ks	4252
USco-160707.7-192715	Keck	36	Brg	4256
USco-160801.4-202741	Pal	56.64	Ks	4252
Usco-160823.2-193001	Keck	32	Brg	4257
USco-160823.8-193551	Keck	32	Brg	4257
USco-160825.1-201224	Keck	32	Brg	4256
USco-160900.7-190852	Pal	56.64	Ks	4252
USco-160908.4-200928	Keck	32	Brg	4256
USco-160916.8-183522	Keck	32	Brg	4256
USco-160954.4-190654	Keck	32	Brg	4256
USco-161031.9-191305	Pal	56.64	Ks	4252
USco-161115.3-175721	Keck	32	Brg	4257
USco-161347.5-183459	Keck	32	Brg	4256

all cases, the AO speckles fall at least a magnitude below our adopted limits.

Finally, the NIRC2 images were distortion-corrected using new high-order distortion solutions (P.B. Cameron, in prep) that deliver a significant performance increase as compared to the solutions presented in the NIRC2 pre-

ship manual[1]; the typical absolute residuals for bright, well-resolved stars are $\lesssim 1$ mas in narrow camera mode. The PHARO images were distortion-corrected using the solution derived by Metchev (2005), with fractional uncertainties in relative astrometry of $\sim 0.15\%$. These uncertainties limit our astrometry for most close, well-resolved binary systems. The uncertainty for wider ($\gtrsim 2$-$3''$) pairs seems to be driven by variation due to differential tilt jitter, while the uncertainty for close blended pairs is driven by our ability to accurately model the single-star PSF.

3.4. Stellar and Companion Properties

Stellar properties can be difficult to estimate, particularly for young stars, since pre-main-sequence stellar evolutionary models are not well-calibrated. The mass of a given sample could be systematically uncertain by as much as 20% (e.g. Hillenbrand & White 2004), and individual masses could be uncertain by factors of 2 or more due to unresolved multiplicity or the intrinsic variability that young stars often display (from accretion or rotational modulation of star spots). This suggests that any prescription for determining stellar properties should be treated with caution.

We estimated the properties of all of our sample members using the methods described in Kraus & Hillenbrand (2007a). This procedure combines the 5 Myr isochrone of Baraffe et al. (1998) and the temperature scales of Schmidt-Kaler (1982) and Luhman et al. (2003) to directly convert observed spectral types to masses. Relative properties (mass ratios q) for all binaries in our sample were calculated by combining these isochrones and temperature scales with the empirical NIR colors of Bessell & Brett (1998) and the K-band bolometric corrections of Leggett et al. (1998) to estimate q from the observed flux ratio ΔK. We also used these techniques to estimate masses for all of our sample members, which we list in Tables 1 and 2.

For all binary systems, we have adopted the previously-measured (unresolved) spectral type for the brightest component and inferred its properties from that spectral type. This should be a robust assumption since equal-flux binary components will have similar spectral types and significantly fainter components would not have contributed significant flux to the original discovery spectrum. Projected spatial separations are calculated assuming the mean distance of Upper Sco, 145 ± 2 pc (de Zeeuw et al. (1999). If the total radial depth of Upper Sco is equal to its angular extent ($\pm 8^o$ or ± 20 pc), then the unknown depth of each system within Upper Sco implies an uncertainty in the projected spatial separation of $\pm 14\%$. The systematic uncertainty due to the uncertainty in the mean distance of Upper Sco is negligible in comparison ($\lesssim 2\%$).

Finally, the sensitivity limits for some of our sample members extend to the bottom of the brown dwarf mass range and could potentially encompass the top of the planetary mass range. However, mass estimates for young giant planets are completely uncalibrated and there are ongoing debates regarding their peak and typical luminosities. The models of Baraffe et al. (2003) imply that a survey sensitive to $K \sim 16$ could detect 7-

[1] http://www2.keck.hawaii.edu/realpublic/inst/nirc2/

10 M_{Jup} planets at the distance and age of Upper Sco. However, more detailed models of planet formation by Marley et al. (2007) suggest that the typical luminosity of a young planet could be 1-2 orders of magnitude lower than previously predicted. These models differ primarily in their treatment of the initial conditions; recent models suggest that accretion shocks could dispel much of the initial energy, leading to lower internal entropy and correspondingly lower initial temperatures than the earlier models predicted. We can not currently resolve this controversy, so we only note that our limits on the presence of massive planets should be considered with caution.

4. NEW COMPANIONS IN UPPER SCO

Our aperture mask survey is sensitive to companions with separations between $\sim\lambda/4D$ and $\sim6\lambda/D$ (at Keck) or $\sim4\lambda/D$ (at Palomar), corresponding to separation ranges of $\sim$10-320 mas and $\sim$20-240 mas, respectively. In this separation range, we identified 12 members of Upper Sco which possess a candidate companion at a confidence level of $\gtrsim$99.5% (99.9% per annulus); the other 60 masking sample members appear to be single to within the detection limits we derived in Section 3.2. In Table 5, we list all of our newly-identified candidate companions and report their flux ratios, separations, and position angles. In Table 6, we summarize our derived upper limits as a function of separation for the 60 remaining members of our sample. The detection limits decline rapidly between $\sim\lambda/4D$ and $\sim2\lambda/3D$, but they are relatively flat at larger separations, extending to contrast ratios of $\sim$5.0-6.5 magnitudes at Keck and $\sim$4.5-5.5 magnitudes at Palomar.

The system RXJ1550.0-2312 was observed on separate nights with separate calibrator sets at Keck in order to confirm the accuracy and repeatablity of our measurements. The separations and contrast ratios measured at each epoch agree to within <1 σ, suggesting that our results are repeatable and our assessed uncertainties are valid. We also we note that three of our calibrators appear to have companions. We did not use these observations in our final data calibration, and we report their astrometry in Table 4 for completeness. Finally, we note that the system GSC 06209-00735 has been previously identified as an SB1 by Guenther et al. (2007). The orbital period that they derived (2045±16 d) is consistent with the projected separation (25±5 mas; 3.6±0.7 AU) of our newly-imaged companion, so these detections appear to denote the same companion. Two more astrometric detections should allow us to resolve the orbital parameters which were not determined in the RV orbit ($K2$, i, and Ω) and directly measure the masses of both stars.

In Table 7, we summarize the observed properties of 7 newly-detected binary systems discovered in our snapshot imaging program, three systems which were discovered in our aperture mask survey and subsequently recovered in our imaging data, and 9 known binary systems for which we report updated properties. In Figure 3, we show the corresponding discovery images for our newly-discovered binaries. We do not report any new candidate companions discovered outside a radius of $2''$ or with $K \geq 15$ because of the significant probability that any such companions are background stars. We have previously estimated the density of background

stars brighter than $K \sim 15$ to be ~1 arcmin^{-2} (Kraus & Hillenbrand 2007a), so the expected number of such contaminants inside $\sim3''$ is only ~1. However, there are many background bulge giants with apparent brightness $K \sim$16-17 that could be mistaken for faint wide companions, so an extension of these limits will require second-epoch observations to confirm common proper motion. Finally, we note that 4 of these sources fell near or inside the detection limits of the speckle interferometry survey of Köhler et al. (2000); their nondetection is most likely explained by an unfavorable orbital phase in 1994-1995 and 14 years of orbital motion.

In Table 8, we list the inferred stellar and binary properties for each of our newly-identified binary systems and the binary systems that we collated from the literature. In Figures 4 and 5, we plot the contrast ratio and mass ratio versus the separation of all of our newly-detected companions, plus the corresponding detection limits for apparently single stars. The vast majority of our newly-identified candidate companions sit well above our survey's detection limits, suggesting that they are all valid detections. Their typical flux ratios ($\Delta K \lesssim3$) indicate that they have stellar masses. Both panels of Figure 3 show an obvious dearth of companions with flux ratios $\Delta K \gtrsim3$, corresponding roughly to the substellar mass range. Our survey should have clearly detected any source in this range of parameter space, as has been proven for orbital monitoring of field binaries like GJ 802 (Lloyd et al. 2006; Ireland et al. 2008), so this deficit seems to represent a genuine absence of companions.

Finally, we did not detect any candidate companions near the typical detection limits of our survey, which correspond to 99.9% confidence limits in any single separation bin or $\sim$99.5% across all separation bins. We would expect an average of 0.3 false detections for the 60 targets listed in Table 6, so our nondetection is consistent with the statistical estimate. We did detect four candidate companions with lower confidence levels (99.5-99.9% in their separation bin, corresponding to overall confidence levels of $\sim$97.5%-99.5%). We would only expect to observe $\sim$1.5 false detections with this range of confidence levels, so 4 represents a marginally significant excess. A discussion off this is given in Section 6.3.

5. THE STELLAR SEA

The properties of multiple star systems are important diagnostics for placing constraints on star formation processes. A comprehensive theory of star formation should be able to reproduce the observed separation distribution, mass ratio distribution, and total fraction of binary systems, as well as any mass or environmental dependences of these properties. The mass ratio distribution also plays a critical role in defining the brown dwarf desert since the bottom tail of the distribution represents the upper bound of the desert.

Most recent efforts to model binary formation have typically assumed that stellar and prestellar interactions play a key role in establishing binary properties. The most popular type of model assumes that a cluster of 5-10 protostellar embryos form from a single turbulently fragmenting cloud core (e.g. Kroupa 1995; Sterzik & Durisen 1998; Kroupa & Bouvier 2003; Kroupa et al. 2003; Delgado-Donate et al. 2003; Hubber et al. 2005); these embryos would then undergo mass accretion and
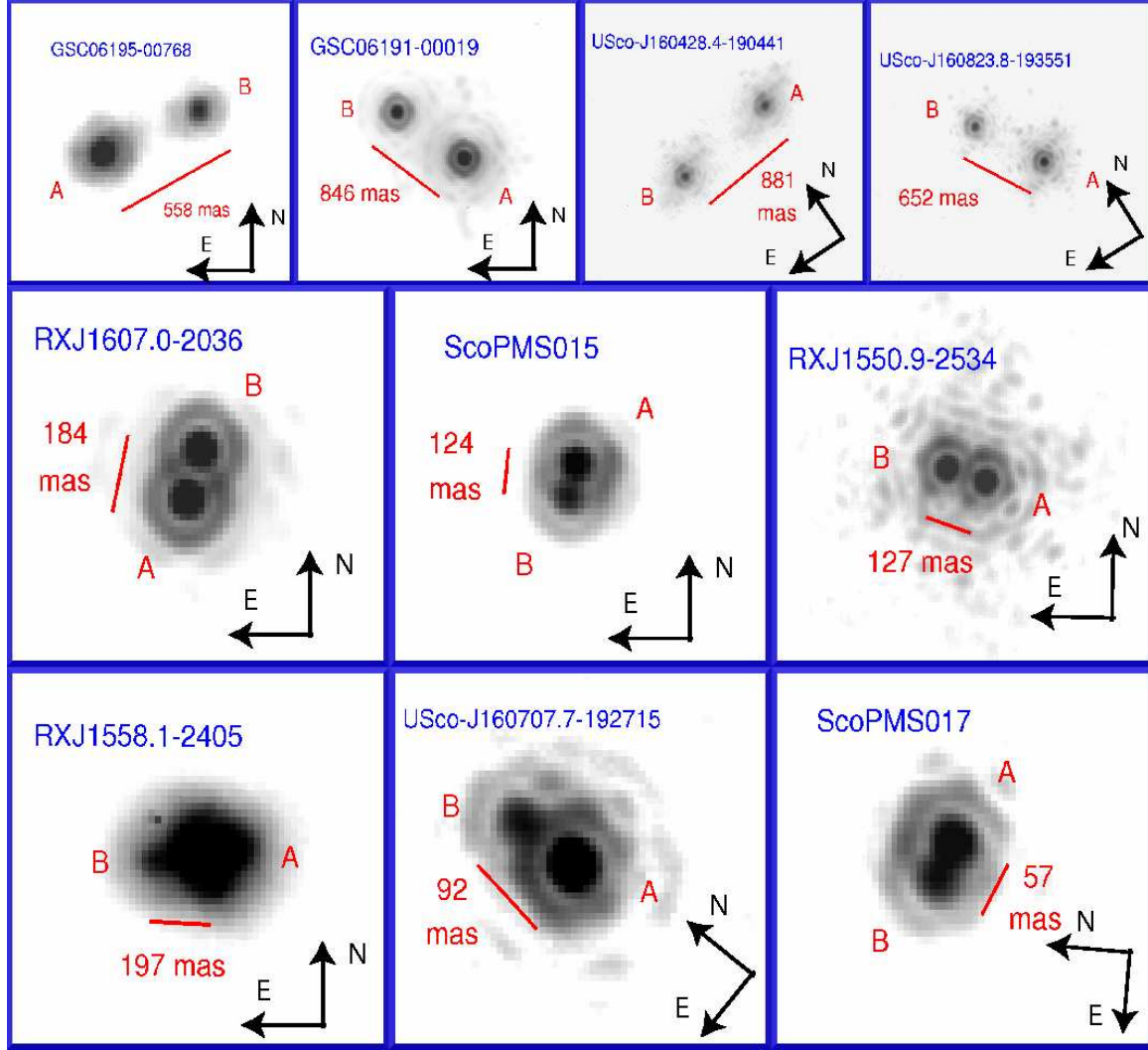
FIG. 3.— Ten new systems that we observed with direct imaging. The top row shows relatively wide (0.5-1.0″) pairs, the middle row shows close, equal-flux pairs that are still easily distinguished, and the bottom row shows three very close or unequal-flux systems that could be difficult to identify with direct imaging alone, but were easily identified with aperture masking.

TABLE 5
COMPANIONS IDENTIFIED WITH THE APERTURE MASK

Primary	Telescope	Δm (mag)	Sep (mas)	PA (deg)
GSC 06209-00735[a]	Palomar	2.44±1.16	24.6±5.2	42.5±3.6
GSC 06764-01305	Keck	2.97±0.01	54.68±0.16	173.76±0.19
GSC 06794-00156	Keck	0.45±0.01	44.30±0.07	230.74±0.08
RXJ1550.0-2312	Keck	0.76±0.01	26.95±0.05	222.13±0.13
RXJ1550.0-2312	Keck	0.76±0.01	26.93±0.04	222.07±0.11
RXJ1558.1-2405	Palomar	2.48±0.09	227.67±1.99	99.23±0.47
RXJ1601.9-2008	Palomar	2.14±0.13	39.31±1.57	217.67±0.59
ScoPMS017	Keck	0.78±0.01	53.86±0.19	68.93±0.20
ScoPMS019	Keck	0.03±0.01	25.40±0.12	113.55±0.62
ScoPMS027	Palomar	0.70±0.03	43.18±0.12	68.63±0.29
USco-160517.9-202420	Keck	0.40±0.07	16.15±0.59	251.12±1.11
USco-160707.7-192715	Keck	2.33±0.01	105.25±0.21	0.90±0.09
USco-161031.9-191305	Keck	2.96±0.02	145.55±0.43	81.63±0.14
Calibrators				
2M1535-2330	Keck	1.35±0.01	92.35±0.17	311.46±0.09
2M1601-2227	Keck	0.64±0.09	249.76±0.5	328.73±0.14
2M1613-2218	Keck	3.97±0.07	93.33±1.04	11.9±0.6

[a] The contrast ratio and separation are highly degenerate at separations this small, but at the least favorable separation, the secondary flux still represents a >7 σ detection.
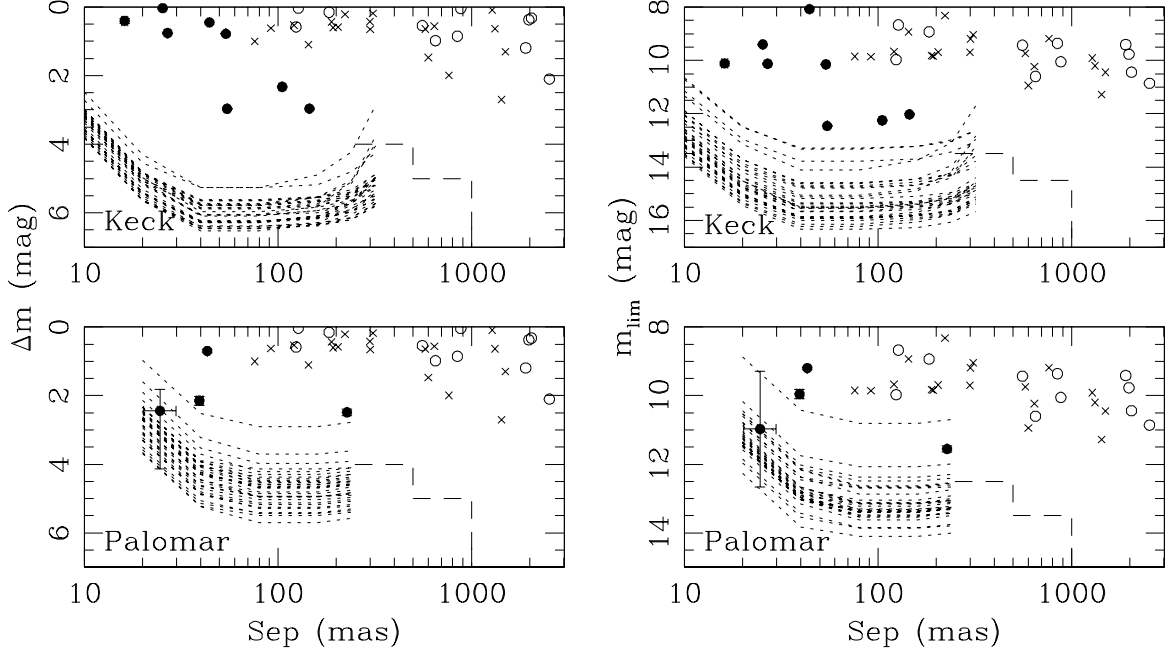
FIG. 4.— Contrast ratio (left) and secondary brightness (right) as a function of separation for our new systems identified via masking (filled circles) and imaging (open circles), plus all known binary systems (crosses). We also show the corresponding aperture-masking detection limits for all apparently single stars in our survey (short-dashed lines) and our adopted sensitivity limits for our imaging data (long-dashed line).
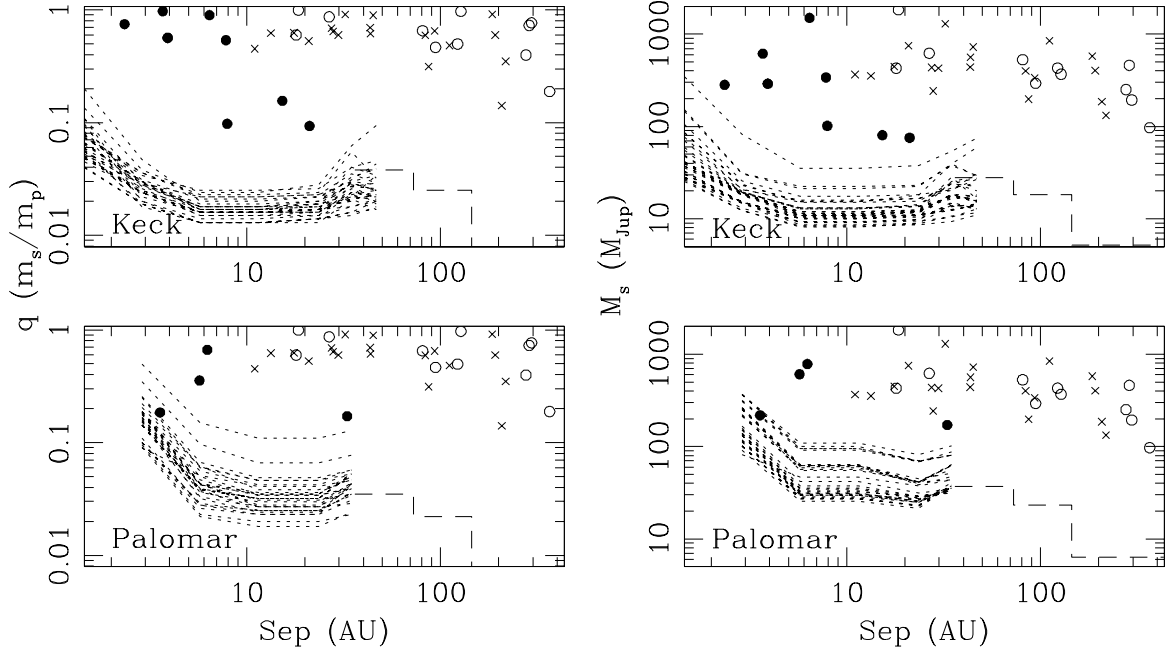

FIG. 5.— As in Figure 4, but showing mass ratio (left) and secondary mass (right) as a function of separation.

TABLE 6
Upper Limits for Undetected Companions

| Primary | Telescope | Δm^{a} | | | | | | $q\ (m_s/m_p)^{\mathrm{a}}$ | | | | | |
		10-20	20-40	40-80	80-160	160-240	240-320	10-20	20-40	40-80	80-160	160-240	240-320
GSC 06191-00552[b]	Palomar	...	3.12	4.71	5.03	4.97	...	...	0.110	0.028	0.025	0.034	...
GSC 06204-00812	Palomar	...	3.23	4.81	5.13	5.03	...	...	0.100	0.029	0.025	0.041	...
GSC 06205-00954	Palomar	...	2.46	4.02	4.50	4.42	...	...	0.157	0.042	0.035	0.050	...
GSC 06208-00834	Palomar	...	2.71	4.30	4.81	4.66	...	...	0.161	0.036	0.030	0.043	...
GSC 06209-01501	Palomar	...	2.62	4.19	4.53	4.49	...	...	0.166	0.039	0.032	0.034	...
GSC 06213-00194	Palomar	...	2.34	3.93	4.43	4.30	...	...	0.185	0.043	0.036	0.048	...
GSC 06213-00306	Palomar	...	2.32	3.89	4.13	4.10	...	...	0.089	0.051	0.041	0.047	...
GSC 06213-00306	Keck	3.23	5.06	5.89	5.80	5.54	5.20	0.098	0.020	0.014	0.015	0.026	0.019
GSC 06213-00306	Palomar	...	3.69	5.24	5.71	5.57	...	...	0.092	0.022	0.018	0.024	...
GSC 06213-01358	Palomar	...	2.66	4.25	4.70	4.58	...	...	0.143	0.038	0.032	0.052	...
GSC 06214-00210	Palomar	...	1.90	3.52	3.98	3.91	...	...	0.250	0.060	0.046	0.053	...
GSC 06214-02384	Palomar	...	2.88	4.45	4.86	4.76	...	...	0.182	0.043	0.028	0.044	...
GSC 06228-01359	Palomar	...	2.70	4.29	4.65	4.57	...	...	0.143	0.038	0.032	0.052	...
GSC 06793-00797	Keck	3.57	5.40	6.25	6.10	5.75	4.94	0.056	0.019	0.013	0.014	0.024	0.023
GSC 06793-00797	Palomar	...	2.14	3.71	4.21	4.10	...	...	0.222	0.062	0.038	0.047	...
GSC 06793-00806	Palomar	...	0.97	2.52	2.90	2.78	...	...	0.499	0.150	0.109	0.128	...
GSC 06793-00994	Palomar	...	3.65	5.23	5.49	5.40	...	...	0.153	0.032	0.024	0.036	...
GSC 06793-01406	Palomar	...	3.06	4.61	4.95	4.82	...	...	0.187	0.056	0.042	0.053	...
GSC 06794-00337	Palomar	...	2.70	4.29	4.60	4.51	...	...	0.190	0.047	0.034	0.039	...
GSC 06794-00480	Palomar	...	1.59	3.23	3.70	3.60	...	...	0.349	0.097	0.066	0.077	...
GSC 06794-00537	Palomar	...	3.31	4.87	5.18	5.08	...	...	0.100	0.026	0.023	0.031	...
RXJ1551.1-2402	Keck	3.07	4.88	5.76	5.63	5.45	5.04	0.073	0.036	0.022	0.023	0.035	0.029
RXJ1557.8-2305	Keck	2.98	4.81	5.78	5.55	5.13	3.96	0.084	0.028	0.018	0.020	0.033	0.039
RXJ1558.2-2328	Keck	3.12	4.93	5.77	5.67	5.42	5.02	0.200	0.047	0.02	0.022	0.031	0.043
RXJ1600.2-2417	Keck	2.72	4.55	5.27	5.18	4.80	4.26	0.109	0.029	0.022	0.023	0.030	0.034
RXJ1600.6-2159	Palomar	...	2.93	4.52	4.95	4.86	...	...	0.177	0.043	0.027	0.042	...
RXJ1600.7-2127	Palomar	...	2.44	4.05	4.47	4.38	...	...	0.187	0.043	0.034	0.040	...
RXJ1601.1-2113	Palomar	...	2.64	4.23	4.68	4.62	...	...	0.143	0.039	0.032	0.053	...
RXJ1602.0-2221	Keck	2.48	4.30	5.26	4.90	4.23	2.86	0.136	0.038	0.024	0.028	0.062	0.094
RXJ1602.8-2401A	Keck	3.06	4.87	5.64	5.57	5.39	4.99	0.108	0.022	0.016	0.016	0.027	0.021
RXJ1602.8-2401B	Palomar	...	2.52	4.08	4.58	4.50	...	...	0.167	0.042	0.031	0.035	...
RXJ1603.6-2245	Palomar	...	3.10	4.65	4.94	4.90	...	...	0.143	0.037	0.027	0.029	...
RXJ1603.9-2031A[b]	Palomar	...	2.86	4.45	4.94	4.86	...	...	0.143	0.033	0.027	0.039	...
RXJ1604.3-2130	Keck	3.57	5.43	6.23	6.15	5.79	5.50	0.060	0.018	0.013	0.013	0.021	0.017
RXJ1605.6-2152[b]	Keck	3.20	5.05	6.09	5.93	5.66	5.24	0.064	0.030	0.017	0.018	0.029	0.025
RXJ1606.2-2036	Keck	2.99	4.83	5.72	5.54	5.05	4.05	0.094	0.025	0.017	0.018	0.022	0.034
RXJ1607.0-2043	Keck	3.15	4.99	5.85	5.78	5.56	5.16	0.066	0.030	0.019	0.020	0.028	0.025
ScoPMS021	Keck	3.37	5.19	6.06	5.94	5.75	5.05	0.081	0.020	0.013	0.014	0.016	0.020
ScoPMS022	Keck	3.14	4.97	5.96	5.84	5.63	5.21	0.066	0.030	0.018	0.019	0.029	0.025
ScoPMS028	Keck	3.02	4.85	5.64	5.54	5.40	4.86	0.078	0.031	0.021	0.022	0.027	0.029
ScoPMS042b	Keck	3.22	5.07	5.85	5.72	5.48	4.99	0.075	0.034	0.025	0.026	0.040	0.034
ScoPMS044	Palomar	...	2.48	4.05	4.38	4.29	...	...	0.182	0.05	0.035	0.053	...
ScoPMS045[b]	Palomar	...	3.28	4.86	5.28	5.23	...	...	0.100	0.028	0.023	0.043	...
ScoPMS048	Palomar	...	2.34	3.93	4.29	4.20	...	...	0.258	0.067	0.049	0.057	...
ScoPMS060	Palomar	...	3.31	4.89	5.26	5.17	...	...	0.206	0.061	0.046	0.057	...
ScoPMS214	Palomar	...	3.58	5.14	5.41	5.30	...	...	0.096	0.023	0.020	0.023	...
USco-155655.5-225839	Keck	3.48	5.31	6.23	6.15	5.95	5.60	0.050	0.025	0.015	0.015	0.018	0.020
USco-160142.6-222923	Keck	3.18	5.00	5.79	5.68	5.52	5.00	0.067	0.027	0.018	0.019	0.023	0.025
USco-160341.8-200557	Keck	3.66	5.50	6.39	6.28	5.88	5.38	0.053	0.028	0.017	0.017	0.027	0.026
USco-160343.3-201531	Keck	3.82	5.65	6.52	6.34	6.05	5.66	0.049	0.024	0.016	0.017	0.021	0.023
USco-160801.4-202741	Keck	3.31	5.13	6.06	6.00	5.71	5.32	0.057	0.026	0.016	0.016	0.024	0.022
USco-160822.4-193004	Keck	3.30	5.13	6.05	5.82	5.08	3.76	0.060	0.029	0.017	0.019	0.040	0.046
USco-160823.2-193001	Keck	3.79	5.64	6.46	6.35	6.20	5.77	0.041	0.019	0.013	0.014	0.016	0.017
USco-160825.1-201224	Keck	3.64	5.46	6.28	6.09	5.91	5.43	0.048	0.024	0.016	0.017	0.021	0.023
USco-160900.7-190852	Keck	3.81	5.63	6.38	6.33	6.14	5.72	0.040	0.019	0.013	0.014	0.015	0.018
USco-160916.8-183522	Keck	3.57	5.40	6.25	6.14	5.97	5.44	0.055	0.029	0.018	0.018	0.020	0.025
USco-160946.4-193735	Keck	3.59	5.42	6.28	6.18	5.98	5.56	0.049	0.024	0.016	0.016	0.022	0.022
USco-160954.4-190654	Keck	3.59	5.42	6.26	6.09	5.68	4.96	0.049	0.024	0.016	0.017	0.030	0.028
USco-161115.3-175721	Keck	3.80	5.63	6.45	6.31	6.15	5.72	0.045	0.024	0.015	0.016	0.023	0.020
USco-161347.5-183459	Keck	2.99	4.83	5.61	5.53	5.33	4.88	0.077	0.036	0.023	0.024	0.055	0.032
USco-161358.1-184828	Keck	3.72	5.56	6.45	6.38	6.19	5.80	0.051	0.024	0.016	0.017	0.018	0.021
V1149 Sco	Palomar	...	3.49	5.06	5.43	5.35	...	...	0.154	0.038	0.025	0.035	...

[a] The range of each separation bin is reported in units of mas, and the corresponding detection limits are reported in terms of δm or q. [b] We detected candidate companions at lower confidence (97.5-99.5%) for these four sources; we plan to obtain additional observations to confirm or disprove them.

TABLE 7
Companions Identified with Direct Imaging

Name	Telescope	Δm (mag)	Sep (mas)	PA (deg)
New				
GSC 06191-00019	Palomar	0.85±0.01	845.8±1	58.0±0.1
GSC 06195-00768	Palomar	0.54±0.01	558±1	292.1±0.3
RXJ1550.9-2534	Keck	0.03±0.01	127.5±1	72.70±0.06
RXJ1558.1-2405[a]	Palomar	1.86±0.03	197±2	98.8±0.3
RXJ1607.0-2036	Palomar	0.15±0.03	183.8±1	344.2±0.3
ScoPMS015	Palomar	0.58±0.02	124.1±1	166.5±0.4
ScoPMS017[a]	Keck	0.65±0.01	57.1±1	68.34±0.11
USco-160428.4-190441	Keck	0.04±0.01	881.1±1	128.13±0.10
USco-160707.7-192715[a]	Keck	1.59±0.01	91.8±1	2.1±0.3
USco-160823.8-193551	Keck	0.98±0.01	651.5±1	64.61±0.11
Known				
GSC 06204-01067	Palomar	2.10±0.01	2528±4	93.04±0.02
GSC 06213-00306	Palomar	2.37±0.01	3186±5	305.11±0.01
GSC 06793-00806	Palomar	1.19±0.01	1907±3	338.81±0.03
GSC 06793-00868	Palomar	0.37±0.01	1981±4	155.29±0.06
RXJ1602.8-2401B	Palomar	2.91±0.02	7198±13	352.22±0.04
ScoPMS048	Palomar	1.76±0.01	3394±5	191.22±0.01
ScoPMS042b	Keck	2.48±0.03	4606±2	6.71±0.03
USco-160908.4-200928	Keck	0.32±0.01	2042±1	139.36±0.07
USco-161031.9-191305	Palomar	3.83±0.02	5775±9	112.66±0.02

[a] Uncertainties are difficult to estimate due to to significant blending of the PSFs. The values and uncertainties from the aperture-masking detection in Table 5 should be used for this system.

TABLE 8
Companion Properties

Name	Sep (AU)	q (m_s/m_p)	M_{prim} ($M_\odot$)	M_{sec} ($M_\odot$)	Source
GSC 06191-00019	122.6	0.50	0.82	0.41	Palomar-Imaging
GSC 06195-00768	80.9	0.65	0.77	0.50	Palomar-Imaging
GSC 06204-01067	366.6	0.19	0.49	0.09	Palomar-Imaging
GSC 06209-00735	3.6	0.18	1.12	0.21	Palomar-Masking
GSC 06213-00306	462.0	0.15	0.87	0.13	Palomar-Imaging
GSC 06214-00210	318.6	0.02	0.60	0.011	Palomar-Imaging
GSC 06764-01305	7.9	0.10	0.99	0.10	Keck-Masking
GSC 06780-01061	217.5	0.35	0.36	0.13	Kraus & Hillenbrand (2007)
GSC 06793-00569	207.4	0.14	1.25	0.18	Metchev (2005)
GSC 06793-00806	276.5	0.40	0.60	0.24	Palomar-Imaging
GSC 06793-00819	32.2	0.91	1.35	1.23	Metchev (2005)
GSC 06793-00868	287.3	0.73	0.60	0.44	Palomar-Imaging
GSC 06794-00156	6.4	0.90	1.59	1.43	Keck-Masking
RXJ1550.0-2312	3.9	0.56	0.49	0.28	Keck-Masking (1)
RXJ1550.0-2312	3.9	0.56	0.49	0.28	Keck-Masking (2)
RXJ1550.9-2534	18.5	1.00	1.75	1.74	Keck-Imaging
RXJ1558.1-2405	33.0	0.17	0.95	0.16	Palomar-Masking
RXJ1558.1-2405	28.6	0.25	0.95	0.23	Palomar-Imaging
RXJ1600.5-2027	27.4	0.69	0.60	0.41	Köhler et al. (2000)
RXJ1601.7-2049	29.7	0.60	0.68	0.41	Köhler et al. (2000)
RXJ1601.8-2445	11.0	0.45	0.77	0.35	Köhler et al. (2000)
RXJ1601.9-2008	5.7	0.36	1.62	0.58	Palomar-Masking
RXJ1602.8-2401B	1043.7	0.10	0.95	0.10	Palomar-Imaging
RXJ1602.9-2022	45.0	0.90	0.77	0.69	Köhler et al. (2000)
RXJ1603.9-2031B	17.6	0.63	0.68	0.43	Köhler et al. (2000)
RXJ1606.6-2108	185.5	0.91	0.60	0.55	Köhler et al. (2000)
RXJ1607.0-1911	86.9	0.31	0.60	0.19	Köhler et al. (2000)
RXJ1607.0-2036	26.7	0.87	0.68	0.59	Palomar-Imaging
ScoPMS005	111.1	0.48	1.66	0.80	Köhler et al. (2000)
ScoPMS013	13.3	0.62	0.54	0.34	Köhler et al. (2000)
ScoPMS015	18.0	0.60	0.68	0.41	Palomar-Imaging
ScoPMS016	192.0	0.60	0.64	0.38	Köhler et al. (2000)
ScoPMS017	7.8	0.54	0.60	0.32	Keck-Masking
ScoPMS017	8.3	0.59	0.60	0.35	Keck-Imaging
ScoPMS019	3.7	0.97	0.60	0.58	Keck-Masking
ScoPMS020	28.0	0.64	0.36	0.23	Köhler et al. (2000)
ScoPMS023	43.5	0.61	0.87	0.53	Köhler et al. (2000)
ScoPMS027	6.3	0.66	1.12	0.74	Palomar-Masking
ScoPMS029	93.2	0.65	0.49	0.32	Köhler et al. (2000)
ScoPMS031	83.8	0.59	0.64	0.38	Köhler et al. (2000)
ScoPMS042a	43.4	0.70	0.60	0.42	Köhler et al. (2000)
ScoPMS048	492.1	0.30	1.35	0.40	Palomar-Imaging
ScoPMS052	20.9	0.53	1.35	0.71	Metchev (2005)
Usco-160428.4-190441	127.8	0.97	0.36	0.35	Keck-Imaging
USco-160517.9-202420	2.3	0.75	0.36	0.27	Keck-Masking
USco-160707.7-192715	15.3	0.16	0.49	0.08	Keck-Masking
USco-160707.7-192715	13.3	0.28	0.49	0.14	Keck-Imaging
USco-160823.8-193551	94.5	0.46	0.60	0.28	Keck-Imaging
USco-160908.4-200928	296.1	0.77	0.24	0.18	Keck-Imaging
USco-161031.9-191305	21.1	0.09	0.77	0.07	Keck-Masking
USco-161031.9-191305	837.4	0.04	0.77	0.03	Palomar-Imaging

NOTE. — Typical uncertainties in separations are ∼15% and result from the unknown depth of each system within the association. The uncertainties in masses are dominated by systematic errors, including a global zero-point uncertainty of ∼20% and individual uncertainties of as much as ∼100% due to the possibility of further unresolved multiplicity. The mass ratio estimates should be more precise (∼5-10%) since many systematics (distance, age, extinction, and zero-point shifts) are cancelled, but they are still vulnerable to large systematic errors due to unresolved multiplicity.

dynamical evolution to form single stars and stable multiple systems. However, other stellar properties place strong limits on the rate of early dynamical evolution. Close stellar encounters would tend to dissipate or truncate disks, with smaller stars having fewer and shorter-lived disks, but there is no evidence for this trend (e.g. White & Basri 2003; Luhman 2004; Scholz et al. 2006). Dynamical encounters might also eject lower-mass stars and brown dwarfs, but no such ejected population is seen (Luhman 2006), though some models suggest that strong ejections might be rare (Bate & Bonnell 2005). Finally, any dynamically active environment would truncate the

stellar binary separation distribution for all stars in the association. The absence of low-mass wide binaries has often been interpreted as a sign of this process, but this absence is seen even in environments where the wide binary frequency is very high for solar-mass stars (Kraus & Hillenbrand 2007a), so it may have another explanation.

Modeling efforts that concentrate on other binary formation processes have not advanced sufficiently to make any rigorous prediction. These processes, which are summarized by Goodwin et al. (2007), include fragmentation of massive circumstellar discs, the role of magnetic support in prestellar cores, and fission of quasi-static ro-
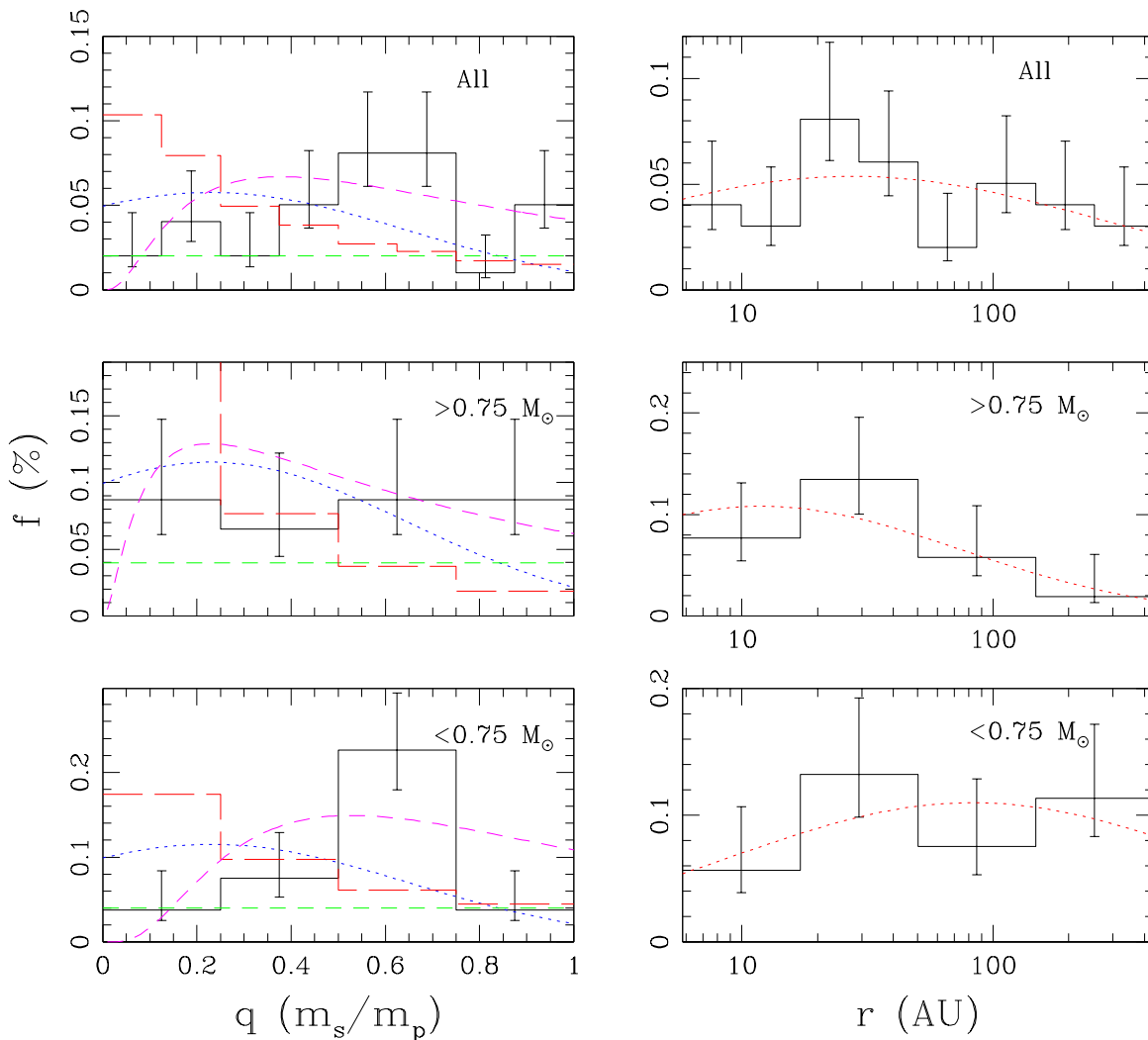
FIG. 6.— The mass ratio distributions (left) and separation distributions (right) for all stars in our sample (top), the more massive half (FGK stars; $M > 0.75\ M_\odot$; middle), and the less massive half (M stars; $M < 0.75\ M_\odot$; bottom). On the left, we overplot several suggested mass functions: a truncated Gaussian distribution (blue dotted), a constant distribution (green dashed), a distribution of companions drawn from the IMF (red long-dashed), and the best-fit log-normal distribution (magenta dashed). On the right, we overplot the best-fit lognormal distribution (red dashed) for each subsample.

tating cores. All of these processes are more significant for isolated cores than for the dynamically-active turbulent fragmentation scenario discussed above, so the limits on dynamical activity of young stars suggest that they should be considered in more detail in the future.

Given the absence of theoretical predictions, we are left only with empirical comparisons to other samples. Previous field multiplicity surveys (DM91; Fischer & Marcy 1992, hereafter FM92; Reid & Gizis 1997, hereafter RG97) have suggested a range of possible results for the separation distribution, mass ratio distribution, and total frequency of binary systems. We will compare our results to these surveys and to the expected result if binary companions are drawn from an IMF. None of these explanations produce an acceptable fit for our mass ratio distribution, so the next step is to test other analytic distributions. Our number statistics do not support strong constraints on this analysis yet, so we will limit our analysis to a single functional form (the log-normal distribution) until we conclude the second half of our survey, an examination of young stars in Taurus.

Finally, we note that two of the systems among our sample (USco-160428.4-190441 and USco-160825.1-201224) would have fallen below the optical flux limit of our sample ($R \leq 14$, imposed by the AO system) if the primaries were single. Including these systems in our statistical analysis would bias our results toward higher binary frequencies, so we have omitted them from our subsequent analysis. There is also an opposing effect due to the inclusion of unresolved binary pairs (which we identify as single stars) that would be omitted by the same criterion if we knew they were binaries. We obviously can't identify these systems, so we only note that the effect should be small. If the binary frequency at small separations is ~10-20% and the mass ratio distribution is similar to the distribution we observe, then no more than 1-2 unresolved systems should be included as "single stars". This systematic bias should not be significant compared to the statistical uncertainties in our results. We also note that our entire analysis must implicitly adopt the assumption that the mass ratio distribution and separation distribution are uncorrelated over the survey's separation range. This assumption has not been rigorously tested, but a simultaneous investigation

TABLE 9
Binary Mass Ratio Distributions

Distribution	Masses	χ^2	P	D_{KS}	P
Gaussian	All	21.2	0.007	0.35	0.00025
	High	5.1	0.28	0.34	0.047
	Low	13.6	0.009	0.41	0.0016
Constant (16%)	All	31.9	0.0001	...	...
	High	11.5	0.021	...	...
	Low	18.3	0.0011	...	...
Constant (35%)	All	11.4	0.18	0.19	0.14
	High	0.17	0.997	0.18	0.67
	Low	11.1	0.025	0.24	0.17
IMF	All	37.0	0.000005	0.46	0.0000004
	High	14.0	0.003	0.52	0.0003
	Low	21.3	0.00009	0.44	0.0005
Log-normal	All	9.7	0.14	0.15	0.41
	High	1.5	0.47	0.21	0.49
	Low	7.6	0.022	0.22	0.23

of both parameters would require a far larger sample.

5.1. *The Mass Ratio Distribution*

Observations of field stars have suggested that the mass ratio distribution is strongly dependent on mass. DM91 showed that F and G stars have mass ratio distributions biased toward inequal masses, roughly consistent with a truncated gaussian distribution (albeit with few constraints for $q < 0.1$). By contrast, FM92 and RG97 found a distribution for early M dwarfs that is roughly flat, and numerous surveys have shown that the distribution for late-M dwarfs and brown dwarfs is biased toward equal masses ($q \gtrsim 0.7$; Close et al. 2003; Bouy et al. 2003; Burgasser et al. 2003). However, these surveys have all studied old field populations. Simulations show that dynamical evolution is typically not significant once a star enters the field (e.g. Weinberg et al. 1987), but a large fraction of stars are thought to be drawn from dense cluster environments (like the Orion Nebula Cluster or the Pleiades), so their properties could have been shaped by significant dynamical evolution in their natal environment. This suggests that primordial binary properties could differ significantly from those of their older brethren.

In the left side of Figure 6, we plot histograms of the mass ratio distribution for our entire sample of 99 stars, only the higher-mass stars (46 FGK dwarfs, representing masses $\gtrsim 0.7\ M_\odot$), and only the lower-mass stars (55 M dwarfs, representing masses $\lesssim 0.7\ M_\odot$). The mass ratio distributions are plotted for projected separations of 0.04-3.0″ (6-435 AU), where the inner bound is defined by the inner limit for our survey to be sensitive to $q \sim 0.04$ and the outer bound is defined by the field star contamination rate predicted for Upper Sco binaries by Kraus & Hillenbrand (2007a). All of the number statistics are only moderately significant, but they still suffice for placing limits on the range of functional forms for the primordial mass ratio distribution.

In all three cases, our survey's mass ratio distribution is not strongly inconsistent with a constant distribution, so our ability to test more complex functional forms is limited. However, our data will suffice to test previously-suggested functions. To this end, we have compared our results to three distributions: a Gaussian distribution like that suggested by DM91, a constant distribution like

that suggested by FM92, and a distribution which was assembled by assuming stars are randomly drawn from the IMF of Upper Sco. None of these functions feature a low-mass cutoff that could explain the brown dwarf desert, so we have also conducted preliminary tests of a new functional form: the log-normal distribution. Our constraints on this distribution are not very stringent, but they allow some preliminary conclusions. We will summarize the results for each of these tests in the following subsections, and we report the goodness of fit statistics (as measured with χ^2 and Kolmogorov-Smirnov tests) in Table 9. The Kolmogorov-Smirnov test is more sensitive in cases where the bin size is a significant fraction of the total range of parameter space or when the trial distribution function changes rapidly accross a bin, so all of our conclusions are based on its results.

5.1.1. *The Gaussian Distribution*

DM91 found that the mass ratio distribution for field F and G dwarfs could be well-fit by a Gaussian distribution centered at low q values ($\mu = 0.23$, $\sigma = 0.42$). Their survey was not sensitive to substellar companions ($q < 0.1$), but if this functional form is valid, it suggests that substellar companions should be very common ($f \sim 10\%$, with 4% falling in our survey's separation range). However, there are no physical motivations for assuming that an arbitrarily chosen segment of a Gaussian function (-0.5σ to $+2.0\sigma$) should predict the mass ratio distribution, so any similarity may be a coincidence. In the three left-hand panels of of Figure 6, we plot the q distribution suggested by DM91 with a blue dotted line. This distribution was originally defined for all separations, but DM91 found that only 40% of their systems fell within our survey's separation range, so we have scaled their function by this amount. This ensures that the overall binary frequency and the shape of the distribution are directly comparable.

Visual inspection shows that our full sample's q distribution is more biased toward equal-mass companions than that of DM91, an observations that is supported by goodness-of-fit tests. This level of disagreement could be a result of our wider mass range than DM91's sample since lower-mass binary systems are thought to have mass ratios that are not as biased toward low masses. The relative levels of agreement for our high-mass and low-mass subsamples support this assessment; the high-mass subsample is only somewhat inconsistent with the DM91 distribution, while the low-mass subsample is very significantly inconsistent.

5.1.2. *The Constant Distribution*

A field binary survey by FM92 found that the mass ratio distribution for field early M dwarfs seemed to be better fit by a flat distribution of mass ratios for $q \gtrsim 0.4$. RG97 found that this flat distribution extends to much lower mass ratio distributions for M dwarfs, though they also suggested the existence of a possible peak near unity ($q \gtrsim 0.8$). As with the Gaussian distribution, a flat distribution would suggest that substellar companions are not uncommon relative to stars, but these survey were not sensitive enough to actually detect most brown dwarf secondaries. Their total binary fractions ($20^{+7}_{-5}\%$ for $q > 0.4$ or $16^{+7}_{-4}\%$ for all q, respectively, in this separation range) are marginally inconsistent, but the RG97

sample (which is more rigorously volume-limited) contains 17 of the 37 binary systems considered by FM92, so we will adopt their value. In the three left-hand panels of Figure 6, we plot the flat q distribution suggested by RG97 with a green dashed line.

Visual inspection suggests that a constant distribution might be more appropriate for our sample's q distribution than the DM91 Gaussian distribution. However, the flat distribution of RG97 appears to fall systematically too low for the full sample and both subsamples, yielding high χ^2 values. If we renormalize the flat distribution to match our overall binary frequency ($36^{+5}_{-4}\%$), we find much better agreement. The corresponding Kolmogorov-Smirnov tests, which only measure the cumulative density function and implicitly include our renormalization, also find that a constant distribution is consistent or perhaps marginally inconsistent. We also note that we found no clear evidence of an excess of equal-mass binaries; the 2-sigma upper limit in the highest-mass bin of our entire sample ($q > 0.875$) is $f < 11.4\%$.

5.1.3. A Distribution Drawn from the IMF

Some theories also suggest that binary companions could be drawn randomly from the IMF. This idea used to be popular since it could be naturally explained as a result of random pairing and because previous results were moderately consistent, but it has fallen out of favor as the role of dynamical interactions has been increasingly constrained. However, an IMF could still be valid for wide binaries (which may form during the turbulent fragmentation of a large cloud core) and it is not clear where this regime ends and where the binary fragmentation of a collapsing protostar begins. This suggests that it would be prudent to test the validity of an IMF-based q distribution. We adopted our IMF (hereafter the companion mass function, or CMF) from the spectroscopic membership surveys of Preibisch et al. (1998, 2002), and Slesnick et al. (2006a, 2007); this IMF can be described by a broken power law, $\Psi(M) = dN/dM \propto M^{-\alpha}$, where $\alpha = -2.8$ for $0.6 < M < 2.0\ M_\odot$, $\alpha = -0.9$ for $0.15 < M < 0.6\ M_\odot$, and $\alpha = -0.6$ for $0.02 < M < 0.15\ M_\odot$.

We derived the expected q distribution for our sample by assuming that every binary primary had a companion randomly drawn from the lower-mass regime of the CMF. Most implementations of this process use Monte Carlo simulations to draw a suitable population from the CMF, but our CMF is defined as a simple analytic function, so we chose to directly convert it into a q distribution: $dN/dq = (dN/dM_{sec})(dM_{sec}/dq) \propto \Psi(qM_{prim})/M_{prim}$, where the full distribution $f(q)$ is the normalized sum of all functions dN/dq as defined for each binary primary. In the three left-hand panels of Figure 6, we plot our IMF-based q distribution with a red long-dashed line. Unlike the previous two distributions, our IMF-based distribution is fundamentally different for our entire sample and for each subsample since they represent different sets of primary masses.

The bottom-heavy nature of the IMF suggests that of all sources with masses $\lesssim 1\ M_\odot$, approximately 1/4 should be substellar and many of the rest should fall at the very bottom of the stellar mass range. This distribution disagrees very significantly with our results, and all statistical tests conclusively rule out the possibility that the companions in our sample might have been randomly drawn from the IMF.

5.1.4. A Parameterized Log-Normal Distribution

As well as simply testing fixed distributions, we can use Bayesian analysis to draw conclusions about the most likely models from a class of distributions. We chose distributions that are log-normal in q (base-10), with a mean at $q = 1$. We chose this distribution because it is based on the following ad-hoc model: beginning with two equal-mass cores, we accrete matter stochastically onto the two cores such that the mean accretion rate onto each core is proportional to the core mass. Applying the central limit theorem to the logarithm of the core mass ratio, we arrive at a log-normal distribution in q. This distribution also has the important property that the functional form is the same in $1/q$ as in q, meaning that it does not matter whether the "primary" or "secondary" star is used as the reference for calculating q. Amongst differentiable q distributions, only distributions that have an asymptotic power-law slope of -1 at $q = 1$ can be written so that they have this property. This distribution has a corresponding probability density function:

$$f(q) = \exp(-\log(q)^2/2\sigma^2)/q. \qquad (1)$$

The likelihood function is then given by:

$$L(\{q_i\}|\sigma) = \Pi_i \frac{\exp(-\log(q_i)^2/2\sigma^2)/q_i}{\int_{0.04}^{1.0} \exp(-\log(x)^2/2\sigma^2)/x\,dx}. \qquad (2)$$

The normalization in this equation explicitly includes our lower limit for q. Using a uniform prior on σ, we find that the best fit value of σ is $0.428^{+0.059}_{-0.049}$. This is our best fit distribution of all tested distributions, and predicts that only 1.2% of all companions are brown dwarfs in our separation range (meaning $q < 0.08$ here). It reproduces the peak in the companion distribution at $q \sim 0.4$ similar to that seen by DM91, but without the lack of near equal-mass companions predicted by their preferred distribution.

The low-mass subsample has a best fit value of σ of $0.347^{+0.063}_{-0.049}$, and the high-mass subsample has a best fit σ of $0.528^{+0.148}_{-0.092}$. These values of σ are significantly different at the 96% level. This demonstrates that the lower mass subsample prefers more equal-mass companions to the higher mass subsample, consistent with results for low-mass binaries in the field. We have plotted all three best-fitting log-normal distributions in the right-hand panels of Figure 6 (magenta dashed line).

5.2. The Binary Separation Distribution

Field surveys have also suggested that the separation distribution depends strongly on mass; the shape seems to be log-normal for a wide range of masses, but the mean and maximum separations decline with decreasing mass. DM91 found that the separation distribution for solar-mass stars has a mean separation of $\sim$30 AU and some binaries as wide as 10^4 AU. FM92 and RG97 found that early M binaries have a mean separation which is marginally consistent (4-30 AU), but few have separations $\gtrsim 10^3$ AU. Finally, recent surveys have shown that late M dwarfs and brown dwarfs have very small mean

and maximum separations (4 and 20 AU, respectively; Close et al. 2003; Bouy et al. 2003; Burgasser et al. 2003). As we described above, many field stars formed in denser environments, so there has probably been some dynamical evolution that disrupted wide binaries. However, surveys of older clusters (e.g. Patience et al. 2002) suggest that the old binary population is only severely depleted by intra-cluster dynamical interactions at separations of $\gtrsim$100-200 AU. This suggests that only the outer edge of our sample's separation distribution should differ significantly from the field.

Interpretation of the companion separation distribution is usually complicated by observational realities. The most meaningful quantity to consider is the distribution of semimajor axes, but the semimajor axis can only be determined as part of an orbital solution. Some authors convert the projected separation for each star into an estimated semimajor axis using a single corrective factor (typically $a = 1.26r$), but this choice is only valid on a statistical level and carries implicit assumptions about the eccentricity distribution that are extrapolated from much shorter-period binaries. Therefore, we choose to report the observed projected separation distribution only. In the right side of Figure 6, we plot histograms of the separation distributions for our entire sample, only the higher-mass FGK stars, and only the lower-mass M dwarfs. This distribution spans separations of 6-435 AU, the range where our survey is sensitive to most brown dwarf companions.

We find that the separation distribution for our sample is consistent with a distribution constant with $\log(r)$, with r the apparent separation on the sky. A one-sided Kolmogorov-Smirnoff test over the separation range 6-435 AU gives $D = 0.13$, with $p = 0.57$. In order to examine what our separation distribution is not consistent with, we have also attempted to fit log-normal distributions over the separation range 6-435 AU, where the likelihood of a particular value of the mean μ and standard deviation σ is given by:

$$ L(\{r_i\}|\mu,\sigma) = \Pi_i \frac{\exp(-(\mu - \log(r_i))^2/2\sigma^2)}{\int_{\log(r_{\min})}^{\log(r_{\max})} \exp(-(\mu - x)^2/2\sigma^2)dx}. \quad (3) $$

As in the previous subsection, the normalization on the denominator is an explicit integral rather than the standard normalization for a Gaussian because of our artificial truncation of the distribution at 6 and 435 AU. We take the prior distribution of μ to be uniform between 0 and 3 (i.e. median separations between 1 and 1000 AU), and the prior distribution of σ to be uniform between 0 and 2. The most likely values of μ and σ are then 1.44 and 1.01 for the entire sample, 1.08 and 0.79 for the high-mass sample, and 1.92 and 0.97 for the low-mass sample. However, integrating over all μ, the most likely value of σ is our upper limit of 2, demonstrating that the data is consistent with an approximately flat distribution. The most important point to come out of this analysis is that the 90% confidence lower limit on σ is 0.94, suggesting that we have detected at most two thirds of the companions in our sample, with the remaining companions being at smaller or greater separations.

The separation distributions for the high and low-mass samples follows the opposite trend to that suggested in

the literature. Our low-mass sample has a median separation of 81 AU, while our high-mass sample has a median separation of 21 AU. This difference is not statistically significant since both distributions are consistent with a constant distribution, and a 2-sided Kolmogorov-Smirnoff test gives a difference statistic $D = 0.30$, with $p = 0.36$. It is interesting, however, that we do not see the trend toward smaller separations with lower masses as seen in field dwarfs (e.g. Allen (2007), who finds $\mu = 0.86$ and $\sigma = 0.28$ for ultracool field dwarfs). We hope to repeat this analysis with more conclusive results after we complete our survey sample.

5.3. *The Total Binary Fraction*

The total binary fraction, representing the integrated separation and mass ratio distributions, provides a useful comparison for different populations. It does not provide any additional information about the binary formation process that is not implicitly included in its component distributions, but it is very useful in other contexts like correcting the IMF for undetected multiplicity or relating the IMF to the prestellar core mass function. Previous surveys suggest that the binary fraction is close to unity for early-type stars, declining to ∼60% for solar-mass stars, and ∼30% for early M stars; in all cases, ∼40-50% of binaries fall within the same separation range as our survey (6-435 AU).

We found binary fractions of 35^{+5}_{-4}% for our entire sample, 33^{+7}_{-5} for our high-mass (FGK) subsample, and 38^{+7}_{-6}% for our low-mass (early M) subsample. The first two results are roughly consistent with those observed in the field, but the second result is significantly higher than the value observed in the field. A survey of wide multiplicity has found that there are only four binaries with separations of 3-30″ among our sample members (Kraus & Hillenbrand 2007a; Kraus & Hillenbrand, in preparation), but there are likely to be a significant number at smaller separations; we discovered some of these binaries inside the nominal completeness limit of our survey, and future RV surveys are likely to uncover many more. If the binary fraction at separations $\lesssim$6 AU is as high in Upper Sco as in the field, then the binary fraction for early M dwarfs in Upper Sco could be as high as is observed for field F-G dwarfs ($\gtrsim$60%).

6. THE FARTHEST SHORE?

In the past 15 years, the search for extrasolar planets has become one of the major goals of the astronomical community. Radial velocity searches have discovered hundreds of planets and allowed us to probe the dynamics of planetary systems (e.g. Marcy et al. 2005), and more recently, transit searches have uncovered dozens of additional planets and allowed us to study their fundamental properties (masses and radii; O'Donovan et al. 2007; Torres 2007). However, the direct observation of extrasolar planetary systems has proven to be an elusive goal. Advances in high-resolution imaging (mostly aimed at speckle suppression) are allowing for increasingly strict upper limits on their existence, but no planetary companions at separations comparable to our own solar system have been directly imaged yet. An intriguing sample of candidate planetary-mass companions have been identified at much wider separations (e.g. Chauvin et al. 2004; Neuhäuser et al. 2005), but their mass and

formation mechanism are still uncertain.

The difficulty of directly detecting extrasolar planets with existing methods suggests that a change of strategy is in order. Previous surveys have typically used spectral or rotational differential imaging (Masciadri et al. 2005; Biller et al. 2007; Lafreniere et al. 2007) to cancel AO speckles, though some surveys have also used direct imaging (typically in the mid-infrared; Kasper et al. 2007) and simply accepted the inherent limits from speckle noise. All of these surveys produce their deepest limits at wide separations ($\gtrsim 0.5''$), so they can only probe the regime of likely planet formation (5-30 AU) for relatively nearby stars ($d \lesssim 30$ pc); even for these stars, existing surveys can not probe deep enough to identify old ($\tau \gtrsim 1$ Gyr) planets, so they must study intermediate-age ($\tau \sim 10$-200 Myr) members of nearby moving groups. By contrast, our survey achieves its deepest limits at much smaller angular separations, so we can probe deeper into the planetary separation regime of nearby moving group members (Ireland & Kraus, in prep) and finally systematically survey the nearest very young associations like Upper Sco.

However, we must include a cautionary note: the fact that we found no high-confidence planetary detections could allow us to place upper limits on the existence of massive Jupiter analogues, but as we have previously described, it could also show that current models severely overestimate the luminosity of young planets. The core-accretion models which predicted this underluminosity have difficulty producing 10 M_{Jup} planets, so it is possible that massive planets are formed via disk fragmentation (which may not suffer this underluminosity). However, all of our subsequent results should be taken with some skepticism. We list all of our detection limits in Table 6, so if the models are updated in the future, it should be trivial to re-analyze our results and produce new limits.

6.1. Modeling the Population of Young Planets

We expect that the planetary population over our range of interest will be described by three parameters: the total frequency f, a power-law mass distribution $dN/dM \propto M^{\alpha}$, and a power-law semimajor axis distribution $dN/da \propto a^{\beta}$. We can place constraints on these parameters by simulating a population of planetary systems for each set of parameters, then convolving this population with our detection limits to determine the level of consistency with our nondetection. Our survey's detection limits can't be directly translated into limits on the planetary population since planets could be obscured by projection effects, so for each simulated planet, we also invoke a random inclination angle, a random true anomaly, and an eccentricity drawn from the approximately Gaussian distribution observed for radial velocity planets (Juric & Tremaine 2007). We note that Juric & Tremaine chose to fit their eccentricity distribution with a Schwartzschild function, but given the uncertainties in the observational statistics, it is not possible to determine whether a Schwartzschild or Gaussian function is more appropriate. We have adopted the more computationally convenient form.

Our specific implementation uses a mass drawn from between 1 and 30 M_{Jup}, a semimajor axis drawn from between 3 and 36 AU, and an eccentricity drawn from a Gaussian distribution between 0.0 and 0.8 with mean $\mu_e = 0.3$ and standard deviation $\sigma_e = 0.3$. We do not directly model the planetary frequency f in our Monte Carlo routine because it can be added analytically. We adopted the upper mass limit (30 M_{Jup}) to match the most massive T Tauri disks at ages of 1-2 Myr (only $\sim 1\%$ of which significantly exceed this mass; Andrews & Williams 2005). After conducting our simulations for a range of values of f, α, and β, we compiled a three-dimensional probability density function $P(f, \alpha, \beta)$ which corresponds to the probability that we would have detected a planet, then extracted three-dimensional confidence surfaces which correspond to the 50%, 90%, 95%, and 99% probabilities that our observations actually would have found no planets.

6.2. Limits on the Population of Young Planets

It is difficult to present a set of three-dimensional confidence surfaces in a two-dimensional medium, so we have chosen to present a selection of two-dimensional slices where we fix one parameter to its current best-estimated value. The statistics of radial velocity surveys have finally become significant enough to suggest possible values of our distribution parameters, so we have adopted these canonical values ($f = 5\%$, $\alpha = -1.05$, $\beta = -1.0$; Marcy et al. 2005) to produce our three confidence plots. The canonical distribution values are derived from radial velocity surveys; they have found the power-law exponents α and β for their sample of (short-period) planets, and they extrapolate that $\sim 5\%$ of their sample members have long-term linear RV trends suggestive of massive long-period planets. The power law exponents may not be valid since many gas giants at small separations are thought to have migrated there, but these values represent the best constraint available.

In the three panels of Figure 7, we present the joint confidence intervals for each pair of values if we fix the third value to the canonical estimate. These results suggest that the canonical planetary distribution can only be ruled out at the $\sim 50\%$ level. This is not a statistically significant level, but it is much better than any previous imaging survey could have achieved. We also find that a much higher planetary frequency is significantly ruled out for most values of α and β; the only values which are consistent require either the mass function or the separation distribution to be very steep, placing most planets in a regime that our survey can not search. Otherwise, we can not rule out significant regions of parameter space. In particular, if the canonical planetary frequency ($f = 5\%$) is accurate, then we can not place any constraints beyond the 70% level on values of α or β. This is a straightforward result of our sample size; with 60 targets, a frequency of 5% suggests that only 3 wide planets exist in our sample. Only unrealistically top-heavy mass or separation distributions would place a significant number of planets in our survey's detection limits.

Finally, we can determine a direct constraint on the total frequency of wide high-mass planets by adopting the canonical values for both α and β, reducing the confidence surface to a confidence interval. If we assume that $\alpha = -1.05$ and $\beta = -1.0$, then there is a 90% probability that $f < 19\%$ and a 95% probability that $f < 24\%$. We can not place similar limits on α and β because these
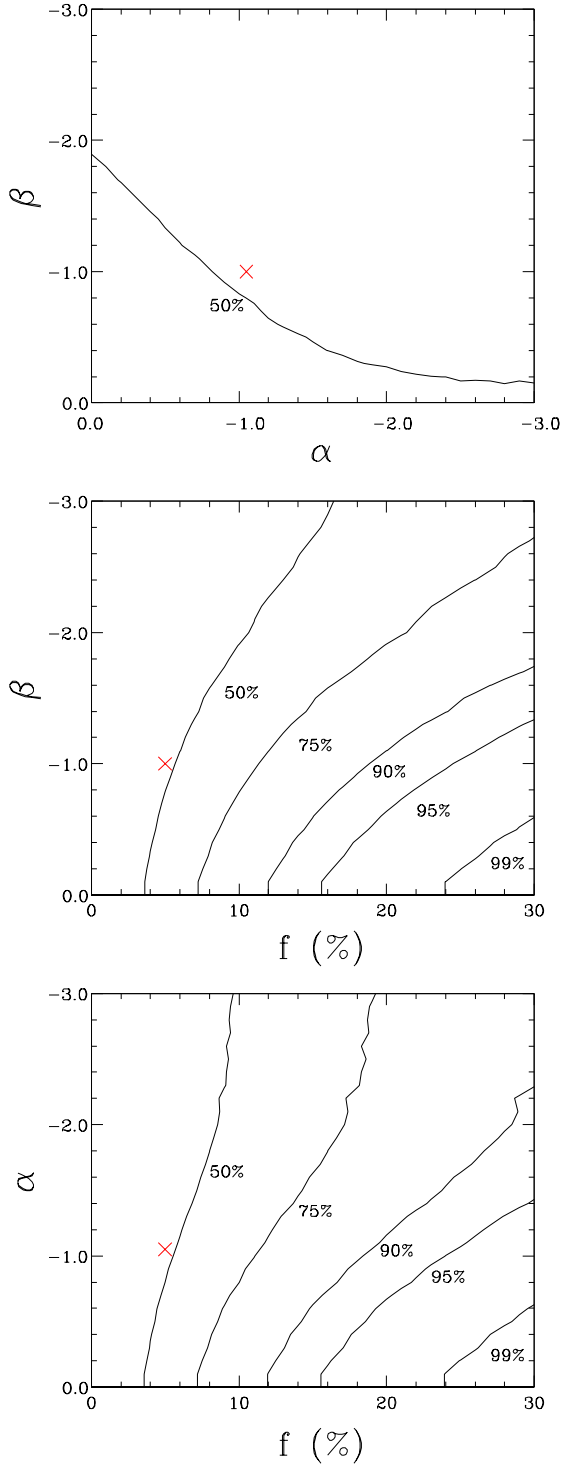
FIG. 7.— Our survey's joint limits on the total giant planet frequency f, the mass function power law α, and the semi-major axis distribution power law β, assuming we fix each parameter at the canonical value suggested by RV surveys (e.g. Marcy et al. 2005): $f = 5\%$ (top), $\alpha = -1.05$ (middle), and $\beta = -1.0$ (bottom). In each case, we also denote the confidence level corresponding to all three canonical values with red crosses.

confidence limits correspond to a total of 2.3 and 3.0 expected detections, respectively; if the total planetary frequency is only $f = 5\%$, then only extremely top-heavy power laws would allow for that many expected detections among our 60 targets.

6.3. An Ocean in the Distance?

Our survey did not identify any faint companions at a confidence level of $\gtrsim 99.5\%$, but it did identify four faint candidate companions at confidence levels of 97.5% to 99.5%. Based on our total sample size (60 targets), the expected number of spurious detections with a confidence level >97.5% is only ~1.5; according to Poisson statistics, the probability of identifying 4 or more of these spurious detections is only 7%, so this seems to represent a marginally significant excess. We will try to obtain followup observations for each marginal detection in the upcoming observing season; given their faintness, any genuine companion in this group could represent the first directly-imaged massive Jupiter analogue.

7. HOW ARID IS THE BROWN DWARF DESERT?

Many multiplicity surveys suggest that the binary companion mass function declines as it enters the brown dwarf mass range, and all results from RV surveys suggest the same for the planetary mass function. In light of these results, it is not surprising that brown dwarf companions are uncommon. The interesting question is whether they are more uncommon than predicted by the tails of both mass functions; if so, then this deficit genuinely represents a brown dwarf "desert".

Our results suggest that the stellar mass ratio distribution is constant or at least not biased heavily toward low-mass companions. Given our observed total binary fraction ($35^{+5}_{-4}\%$), a constant mass ratio distribution predicts that ~3.5% of all stars should have a substellar or nearly-substellar companion with $q \leq 0.1$ at separations of 6-435 AU. We have found two such companions ($1.8^{+2.3}_{-0.6}\%$), a result which is entirely consistent with that claim. However, both companions fall at the upper end of this range ($q = 0.10$ and $q = 0.09$), and only one is possibly substellar ($M_{sec} \sim 0.07\ M_\odot$); given the uncertainties inherent to our estimates of stellar properties, it is not inconceivable that both companions could fall in the range $q > 0.1$. This would be consistent with estimates for wide companions to much higher-mass Upper Sco members; Kouwenhoven et al. (2007) found that only 0.5±0.5% of the B and A stars in Upper Sco have substellar companions with separations of 130-520 AU.

Our estimate of the contribution from planetary formation processes is much more uncertain. If the planetary distribution is truly defined by the canonical values given in the literature ($f = 5\%$, $\alpha = -1.05$, and $\beta = -1.0$) and the models describing luminosities of young planets are correct, then our survey would have had a 50% chance of detecting one "planetary" companion of any mass <30 M_{Jup}. This probability would have been higher if the planetary mass function extends beyond 30 M_{Jup} with no cutoff, but even a cutoff at 100 M_{Jup} would imply that our null detection is significant at only ~75%. As a result, we can not state with any confidence that the canonical values are incorrect or that there is any sort of high-mass cutoff in the planetary mass function.

8. SUMMARY

We present the results of a survey for stellar and substellar companions to 82 young stars in the nearby OB association Upper Scorpius. This survey used nonredundant aperture-mask interferometry to achieve typical contrast limits of $\Delta K \sim 5$-6 at the diffraction limit,

revealing 12 new companions that lay below the detection limits of traditional high-resolution imaging; we also summarize a complementary snapshot imaging survey that discovered 7 directly resolved companions. The overall frequency of binary companions ($\sim 33^{+5}_{-4}\%$ at separations of 6-435 AU, including companions reported in the literature) appears to be similar to field stars of similar mass, but the companion mass function appears to be more biased toward equal-mass companions than the equivalent mass function in the field. This result could indicate an environmental or dynamical effect, but our number statistics are not yet sufficient to place strong constraints on its nature.

Our survey limits encompass the entire brown dwarf mass range and we detected two companions with $q \leq 0.1$, a number which is consistent with a flat mass ratio distribution. However, both of these companions have mass ratios near 0.1 and only one has a mass which might fall below the substellar boundary, so we hesitate to rule out the existence of any deficit that might denote a brown dwarf "desert". Our survey's deep detection limits also extend into the top of the planetary mass function; we have not identified any planetary companions at high confidence ($\gtrsim 99.5\%$), but we have identified four candidate companions at lower confidence ($\gtrsim 97.5\%$) that merit additional followup to confirm or disprove their existence. The lack of planets within the brown dwarf mass range also is not a significant proof of the existence of a desert.

Finally, we note that our survey results are extremely encouraging with respect to the potential for future discoveries. We are currently extending our survey efforts to the Taurus-Auriga star forming region and to several nearby moving groups, and this expansion of our sample should make any conclusions much more robust. Our ability to precisely measure astrometry for close (~ 2-3 AU) binary systems could also allow us to measure dynamical masses for many young stars on a timescale of $\lesssim 5$ yr. Finally, achieving similar detection limits for planetary-mass companions in Taurus-Auriga and the nearby moving groups will significantly enhance our limits on the properties of young planets; a similar null detection for our full sample would significantly rule out the canonical values for the planetary distribution function, confirming either that these values are wrong or that evolutionary models significantly overestimate the luminosity (and detectability) of young planets.

9. APPENDIX A: THE DETECTION LIMITS OF NONREDUNDANT APERTURE MASK OBSERVATIONS

For each set of n frames (called a *run*), with $n \geq 8$, we calculate the mean closure phase vector $\bar{\phi}$ and an estimate for the covariance matrix of closure-phase:

$$\hat{C}_r = \frac{\Sigma_i (\phi_i - \bar{\phi})^t (\phi_i - \bar{\phi})}{n-1}. \tag{4}$$

Here ϕ_i is the closure-phase vector calculated for a single frame and ^{t} represents a transpose. The variance in closure-phase calculated by this technique (the diagonal of $\hat{C}_r$) will be called $\hat{\sigma}_r^2$.

Studentizing all statistics was seen as an excessively difficult task, given the high number of dimensions in our data set, the strong correlations between measured

parameters and the need to have fast, automatic fitting routines. In order to limit susceptibility to the lack of a tail in the Gaussian approximation for uncertainties that follow a student's t distribution, we artificially increased the errors on closure phases with the smallest errors. We did this by applying an error cutoff at 2/3 of the median closure-phase error. In the case of closure-phases with equal true errors, this means that we would have artificially increased the uncertainties on 12% of the closure triangles, changing the expected value of reduced χ^2 from 1.4 to 1.24 for $n = 8$, making a smaller difference for large n.

In addition to the error calculated from a single run, we calculated closure-phase uncertainties from the dispersion amongst calibrator observations. We will denote these variances $\hat{\sigma}_c^2$. Where the error calculated from dispersion amongst the calibrators was greater than that given by the standard error of the mean for a single suns, we weighted the error estimates by:

$$\hat{\sigma}^2 = \frac{2\hat{\sigma}_r^2 + (n_c - 1)\hat{\sigma}_c^2}{n_c + 1} \tag{5}$$

After errors were increased by either the scatter amongst calibrators or the closure-phase uncertainty histogram cutoff, the covariance matrix was modified in such a way that the correlation matrix remained unchanged.

After finding the covariance matrix of calibrated closure-phase, we found that in general the errors in its calculation caused excessive noise in calculation of the covariance matrix inverse. For this reason, we first filtered the covariance matrix by fitting a model of the form:

$$\mathrm{Var}(\theta_{ijk}) = \frac{\sigma_f^2}{\langle |V_i V_j V_k| \rangle} + \mathrm{Var}(\theta_i) + \mathrm{Var}(\theta_j) + \mathrm{Var}(\theta_k), \tag{6}$$

and

$$\mathrm{Cov}(\theta_{ijk}, \theta_{jlm}) = \pm Var(\theta_i). \tag{7}$$

$\mathrm{Var}(\theta_i)$ is a model variance of phase for baseline i, which in turn has the form:

$$\mathrm{Var}(\theta_i) = \sigma_i^2 + \alpha(m_{tx} m_{tx}^t + m_{ty} m_{ty}^t). \tag{8}$$

Here σ_i is the intrinsic phase variance of baseline i, α is a free parameter and m_{tx} and m_{ty} are closure-phase modes caused by skewness of the image in x and y directions. This skewness is caused by temporal effects, where in a single exposure, tip/tilt errors can be asymmetrical, with e.g. a single "glitch" where for 10% of the exposure the image is offset by $20\,\mathrm{mas}$. This can be a dominant error term at Palomar, where the tip/tilt mirror is too large to have an adequate correction bandwidth in poor seeing. The $\pm$ in Equation 7 is a $+$ if baseline i is counted in the same direction for both closure-phases, and it is a $-$ if baseline i is counted in opposite directions for both closure-phases.

Finally, in the fitting process, reduced χ^2 was often greater than 1. Although by chance, this should have occured $50\,\%$ of the time if uncertainties were correctly estimated, in practice it occured $\sim 90\,\%$ of the time. A

possible reason for this could be residual systematics differences in sky position or color, despite the care taken to minimise these differences in a single observing block. When this occured, additional systematic closure-phase uncertainties were added so that reduced χ^2 was 1. For determining the confidence level of a null detection, this reduced χ^2 corresponds to the reduced χ^2 for a single star fit, and for determining errors on a non-null detection, this reduced χ^2 corresponds to that for the best binary fit.

Due to the linear dependence of model closure-phases, we calculate χ^2 on a closure-phase vector space with dimensionality equal to the number of independent closure phases, $N_{\rm ind}$. This vector space $V_{\rm ind}$ is formed by projection via a matrix T_p, defined so that the covariance matrix on $V_{\rm ind}$ is a diagonal matrix D:

$$D = T_p C^{-1} T_p^t. \qquad (9)$$

This means that, given a closure phase vector $\phi_{\mathbf{d}}$, the covariance matrix of the linear combination $T_p\phi_{\mathbf{d}}$ is given by the diagonal matrix D. Given model closure phases $\phi_{\mathbf{m}}$ and data $\phi_{\mathbf{d}}$, the value of χ^2 is then given by:

$$\chi^2 = (\phi_{\mathbf{m}} - \phi_{\mathbf{d}})^t T_p^t D T_p (\phi_{\mathbf{m}} - \phi_{\mathbf{d}}) \qquad (10)$$

It is this χ^2 that was minimised when fitting binary functions to closure-phase. The Monte-Carlo procedure was simplified computationally by limiting the fitting prodecure to the high-contrast regime, where closure-phase is a linear function of companion brightness. In this regime, model closure-phases $\phi_{\mathbf{m}}$ were found for each separation and position angle for a fixed contrast ratio R_m, with the fitted contrast ratio given by:

$$R = R_m \frac{\sigma \mathbf{Z^t} D T_p \phi_{\mathbf{m}}}{\phi_{\mathbf{m}}^{\mathbf{t}} T_p^t D T_p \phi_{\mathbf{m}}} \qquad (11)$$

The matrix $\sigma\mathbf{Z}$ is a standard normal vector of length $N_{\rm ind}$, multiplied by the standard errors as calculated in the vector space $V_{\rm ind}$. This equation is relatively simple to derive my minimizing χ^2 where the model closure phase at contrast R is $(R/R_m)\phi_{\mathbf{m}}$.

REFERENCES

Ahmic, M., Jayawardhana, R., Brandeker, A., Scholz, A., van Kerkwijk, M., Delgado-Donate, E., & Froebrich, D. 2007, ApJ, 671, 2074
Andrews, S. & Williams, J. 2005, ApJ, 631, 1134
Ardila, D. et al. 2000, AJ, 120, 479
Allen, P. 2007, ApJ, in press, (arXiv:0707.2064)
Baraffe, I., Chabrier, G., Allard, F., & Hauschildt, P. 1998, A&A, 337, 403
Bate, M. & Bonnell, I. 2005, MNRAS, 356, 1201
Bessell, M. & Brett, J. 1988, PASP, 100, 1134
Biller, B. et al. 2007, ApJS, in press
Bouy, H. et al. 2003, AJ, 126, 1526
Bouy, H. et al. 2006, A&A, 451, 177
Brandner, W. et al. 1996, A&A, 307, 121
Burgasser, A. et al. 2003, ApJ, 125, 850
Carpenter, J. 2001, AJ, 121, 2851
Carson, J. et al. 2005, AJ, 130, 1212
Chabrier, G. et al. 2000, ApJ, 542, 464
Chauvin, G., Lagrange, A., Dumas, C., Zuckerman, B., Mouillet, D., Song, I., Beuzit, J., & Lowrance, P. 2004, A&A, 425, 29
Chiu, K., Fan, X., Leggett, S. K., Golimowski, D. A., Zheng, W., Geballe, T. R., Schneider, D. P., & Brinkmann, J. 2006, AJ, 131, 2722
Close, L. et al. 2003, ApJ, 587, 407
de Zeeuw, P., Hoogerwerf, R., de Bruijne, J., Brown, A., & Blaauw, A. 1999, AJ, 117, 354
Delgado-Donate, E. et al. 2003, MNRAS, 347, 759
Duquennoy, A. & Mayor, M. 1991, A&A, 248, 485
Fischer, D. & Marcy, G. 1993, ApJ, 396, 178
Gizis, J., Kirkpatrick, J.D., Burgasser, A., Reid, I.N., Monet, D., Liebert, J., & Wilson, J. 2001, ApJ, 551, L163
Goodwin, S. & Kroupa, P. 2007, in Protostars and Planets V, ed. B. Reipurth, D. Jewitt, & K. Keil (Tucson: Univ. Arizona Press), 133
Grether, D. & Lineweaver, C. 2006, ApJ, 640, 1051

Hillenbrand, L. & White, R. 2004, ApJ, 604, 741
Houk, N. & Smith-Moore, M. 1988, Michigan Spectral Survey (Ann Arbor: Dept. Astron. UNiv. Mich.),4
Hubber, D. & Whitworth, A. 2005, A&A, 437, 113
Johnson, J. et al. 2006, ApJ, 647, 600
Juric, M. & Tremaine, S. 2007, submitted to ApJ (astro-ph/0703160)
Kim, S., Figer, D., Lee, M., & Oh, S. 2005, PASP, 117, 445
Kirkpatrick, J. D., Reid, I. N., Liebert, J., Gizis, J. E., Burgasser, A. J., Monet, D. G., Dahn, C. C., Nelson, B., & Williams, R. J. 2000, AJ, 120, 447
Köhler, R. et al. 2000, A&A, 356, 541
Kouwenhoven, M.B.N., Brown, A.G.A., & Kaper, L. 2007, A&A, 464, 581
Kraus, A., White, R., & Hillenbrand, L. 2006, ApJ, 649, 306
Kraus, A. & Hillenbrand, L. 2007, ApJ, 662, 413
Kraus, A. & Hillenbrand, L. 2007, ApJ, 664, 1167
Kroupa, P. 1995, MNRAS, 277, 1491
Kroupa, P. & Bouvier, J. 2003, MNRAS, 346, 369
Kroupa, P. et al. 2003, MNRAS, 346, 354
Kunkel, M. 1999, PhDT
Ireland, M., Kraus, A., Martinache, F., Lloyd, J.P., & Tuthill, P.G. 2008, ApJ, in press (arXiv:0801.1525)
Lafreniere, D. et al. 2007, ApJ, in press
Leggett, S., Allard, F., & Hauschildt, P. 1998, ApJ, 509, 836
Lissauer, J. & Stevenson, D. 2007, in Protostars and Planets V, ed. B. Reipurth, D. JEwitt, & K. Keil (Tucson: Univ. Arizona Press), 591
Lloyd, J., Martinache, F., Ireland, M., Monnier, J., Pravdo, S., Shaklan, S., & Tuthill, P. 2006, ApJL, 650, 131
Lohmann, A. W., Weigelt, G., & Wirnitzer, B. 1983, Appl. Opt., 22, 4028
Luhman, K. et al. 2003, ApJ, 593, 1093
Luhman, K. 2004, ApJ, 602, 816
Luhman, K. 2006, ApJ, 645, 676

McCarthy, C., & Zuckerman, B. 2004, AJ, 127, 2871

Marcy, G. & Butler, R. 2000, PASP, 112, 137

Marcy, G., Butler, R., Fischer, D., Vogt, S., Wright, J., Tinney, C., & Jones, H. 2005, Prog. Theor. Phys. Suppl., 158, 24

Marley, M., Fortney, J., Hubickyj, O., Bodenheimer, P., & Lissauer, J. 2007, ApJ, 655, 541

Martin, E. et al. 2004, AJ, 127, 449

Martinache, F., Lloyd, J., Ireland, M., Yamada, R., & Tuthill, P. 2007, ApJ, 661, 496

Masciadri, E., Mundt, R., Henning, Th., Alvarez, C., & Barrado y Navascues, D. 2005, ApJ, 625, 1004

Metchev, S. 2005, PhD thesis(http://etd.caltech.edu/etd/available/etd-08262005-320655/)

Monet, D. et al. 2003, AJ, 125, 984

Naef, D. et al. 2007, A&A, 470, 721

Nakajima, T. et al. 1989, AJ, 97, 1510

Neuhäuser, R., Guenther, E., Alves, J., Huélamo, N., Ott, Th., & Eckart, A. 2003, AN, 324, 535

Neuhäuser, R. & Guenther, E. 2004, A&A, 420, 647

Neuhäuser, R., Guenther, E., Wuchterl, G., Mugrauer, M., Bedalov, A., & Hauschildt, P. 2005, A&A, 435, 13

O'Donovan, F. et al. 2007, ApJ, 663, 37

Patience, J. et al. 2002, AJ, 123, 1570

Pravdo, S. et al. 2006, ApJ, 649, 389

Preibisch, T. et al. 1998, A&A, 333, 619

Preibisch, T., Guenther, E., & Zinnecker, H. 2001, AJ, 121, 1040

Preibisch, T., Brown, A., Bridges, T., Guenther, E., & Zinnecker, H. 2002, AJ, 124, 404

Reid, I. & Gizis, J. 1997, AJ, 113, 2246

Reid, I., Gizis, J., Kirkpatrick, J., & Koerner, D. 2001, AJ, 121, 489

Schmidt-Kaler, Th., "Physical Parameters of the Stars", Landolt-Bornstein Numerical Data and Functional Relationships in Science and Technology, New Series, Group VI, Volume 2b, Springer-Verlag, Berlin, 1982

Scholz, A., Jayawardhana, R., & Wood, K. 2006, ApJ, 645, 1498

Skrutskie, M. et al. 2006, AJ, 131, 1163

Slesnick, C., Carpenter, J., & Hillenbrand, L.2006a, AJ, 131, 3016

Slesnick, C., Carpenter, J., Hillenbrand, L., & Mamajek, E. 2006b, ApJ, 644, 1056

Slesnick, C. PhD thesis

Stephenson, C.B. 1987, ApJ, 300, 779

Sterzik, M. & Durisen, R. 1998, A&A, 339, 95

Stetson, P. 1987, PASP, 99, 191

Torres, G. 2007, ApJL, in press

Tuthill, P. et al. 2000, PASP, 112, 555

Walter, F. et al. 1994, AJ, 107, 692

Weinberg, M., Shapiro, S., & Wasserman, I. 1987, ApJ, 312, 367

White, R. & Basri, G. 2003, ApJ, 582, 1109

Whitworth, A. & Stamatellos, D. 2006, A&A, 458, 817